NUREG/CR–4667
ANL–95/2
Vol. 18

Environmentally Assisted Cracking in Light Water Reactors

Semiannual Report
October 1993 – March 1994

Manuscript Completed: January 1995
Date Published: March 1995

Prepared by
H. M. Chung, O. K. Chopra, R. A. Erck, T. F. Kassner, W. F. Michaud
W. E. Ruther, J. E. Sanecki, W. J. Shack, W. K. Soppet

Argonne National Laboratory
9700 South Cass Avenue
Argonne, IL 60439

Prepared for
Division of Engineering
Office of Nuclear Regulatory Research
U.S. Nuclear Regulatory Commission
Washington, DC 20555-0001
NRC Job Code A2212

Previous Documents in Series

Environmentally Assisted Cracking in Light Water Reactors Semiannual Report April–September 1985, NUREG/CR-4667 Vol. I, ANL-86-31 (June 1986).

Environmentally Assisted Cracking in Light Water Reactors Semiannual Report October 1985–March 1986, NUREG/CR-4667 Vol. II, ANL-86-37 (September 1987).

Environmentally Assisted Cracking in Light Water Reactors Semiannual Report April–September 1986, NUREG/CR-4667 Vol. III, ANL-87-37 (September 1987).

Environmentally Assisted Cracking in Light Water Reactors Semiannual Report October 1986–March 1987, NUREG/CR-4667 Vol. IV, ANL-87-41 (December 1987).

Environmentally Assisted Cracking in Light Water Reactors Semiannual Report April–September 1987, NUREG/CR-4667 Vol. V, ANL-88-32 (June 1988).

Environmentally Assisted Cracking in Light Water Reactors Semiannual Report October 1987–March 1988, NUREG/CR-4667 Vol. 6, ANL-89/10 (August 1989).

Environmentally Assisted Cracking in Light Water Reactors Semiannual Report April–September 1988, NUREG/CR-4667 Vol. 7, ANL-89/40 (March 1990).

Environmentally Assisted Cracking in Light Water Reactors Semiannual Report October 1988–March 1989, NUREG/CR-4667 Vol. 8, ANL-90/4 (June 1990).

Environmentally Assisted Cracking in Light Water Reactors Semiannual Report April–September 1989, NUREG/CR-4667 Vol. 9, ANL-90/48 (March 1991).

Environmentally Assisted Cracking in Light Water Reactors Semiannual Report October 1989–March 1990, NUREG/CR-4667 Vol. 10, ANL-91/5 (March 1991).

Environmentally Assisted Cracking in Light Water Reactors Semiannual Report April–September 1990, NUREG/CR-4667 Vol. 11, ANL-91/9 (May 1991).

Environmentally Assisted Cracking in Light Water Reactors Semiannual Report October 1990–March 1991, NUREG/CR-4667 Vol. 12, ANL-91/24 (August 1991).

Environmentally Assisted Cracking in Light Water Reactors Semiannual Report April–September 1991, NUREG/CR-4667 Vol. 13, ANL-92/6 (March 1992).

Environmentally Assisted Cracking in Light Water Reactors Semiannual Report October 1991–March 1992, NUREG/CR-4667 Vol. 14, ANL-92/30 (August 1992).

Environmentally Assisted Cracking in Light Water Reactors Semiannual Report April–September 1992, NUREG/CR-4667 Vol. 15, ANL-93/2 (June 1993).

Environmentally Assisted Cracking in Light Water Reactors Semiannual Report October 1992–March 1993, NUREG/CR-4667 Vol. 16, ANL-93/27 (September 1993).

Environmentally Assisted Cracking in Light Water Reactors Semiannual Report April–September 1993, NUREG/CR-4667 Vol. 17, ANL-94/26 (June 1994).

DISCLAIMER

Environmentally Assisted Cracking in Light Water Reactors

by

H. M. Chung, O. K. Chopra, R. A. Erck, T. F. Kassner, W. F. Michaud, W. E. Ruther, J. E. Sanecki, W. J. Shack, and W. K. Soppet

Abstract

This report summarizes work performed by Argonne National Laboratory (ANL) on fatigue and environmentally assisted cracking (EAC) in light water reactors (LWRs) during the six months from October 1993 to March 1994. EAC and fatigue of piping, pressure vessels, and core components in LWRs are important concerns in operating plants and as extended reactor lifetimes are envisaged. Topics that have been investigated include (a) fatigue of low-alloy steel used in piping, steam generators, and reactor pressure vessels, (b) EAC of wrought and cast austenitic stainless steels (SSs), and (c) radiation-induced segregation and irradiation-assisted stress corrosion cracking (IASCC) of Type 304 SS after accumulation of relatively high fluence. Fatigue tests have been conducted on A302-Gr B low-alloy steel to verify whether the current predictions of modest decreases of fatigue life in simulated pressurized water reactor water are valid for high-sulfur heats that show environmentally enhanced fatigue crack growth rates. Additional crack growth data were obtained on fracture-mechanics specimens of austenitic SSs to investigate threshold stress intensity factors for EAC in high-purity oxygenated water at 289°C. The data were compared with predictions based on crack growth correlations for wrought austenitic SS in oxygenated water developed at ANL and rates in air from Section XI of the ASME Code. Microchemical and microstructural changes in high- and commercial-purity Type 304 SS specimens from control-blade absorber tubes and a control-blade sheath from operating boiling water reactors were studied by Auger electron spectroscopy and scanning electron microscopy to determine whether trace impurity elements, which are not specified in the ASTM specifications, may contribute to IASCC of solution-annealed materials.

Contents

Figures

Tables

Executive Summary

Fatigue of Ferritic Piping and Pressure Vessel Steels

Plain carbon steels are used extensively in steam supply systems of pressurized and boiling water nuclear reactors (PWRs and BWRs) as piping and pressure vessel materials. The steels of interest for these applications include A106-Gr B and A333-Gr 6 for seamless pipes and A302-Gr B, A508-2, and A533-Gr B plate for pressure vessels. During the present reporting period, fatigue tests have been conducted on A302-Gr B low-alloy steel to verify whether the current predictions of modest decreases of fatigue life in simulated PWR water are valid for high-sulfur heats that show environmentally enhanced fatigue crack growth rates (CGRs) in precracked specimens. This A302-Gr B low-alloy steel contains a high concentration of sulfur (0.027 wt.%) and exhibits increased CGRs in simulated PWR water with <10 ppb dissolved oxygen (DO). Fatigue tests were conducted in air and simulated PWR water, i.e., water containing <0.01 ppm DO, 2 ppm lithium, and 1000 ppm boron, at 288°C and a strain range of ≈0.75% with triangular and sawtooth wave forms. In air and water environments, the results for A302-Gr B steel are in good agreement with the data for A533-Gr B steel. The results indicate only a marginal effect of PWR water on fatigue life, i.e., life of A302-Gr B steel is lower by ≈23% in PWR water than in air at strain rates in tension of 0.4 and 0.004 %/s. Even a 1/8-cycle slow/fast test, with a slow strain rate of 0.0004%/s, shows only a moderate decrease in fatigue life. These results are consistent with data obtained earlier for A106-Gr B carbon steel and A533-Gr B low-alloy steel. The data suggest that even high-sulfur steels suffer only modest decreases of fatigue life in simulated PWR water.

Tests were also conducted on A106-Gr B steel in high-DO water at 288°C and a strain range of ≈0.75% with 5- or 30-min hold periods at peak tensile strain. The results indicate that a tensile hold period decreases fatigue life in high-DO water but not in air. A 5-min hold period is sufficient to reduce fatigue life.

Environmentally Assisted Cracking of Cast Stainless Steels

During this reporting period, fracture-mechanics CGR tests were conducted on 1T-compact tension specimens of Type 316NG and 304 stainless steel (SS) and as-received and thermally aged CF-3 cast SS to investigate threshold stress intensity factors K_{th}^{EAC} for environmentally assisted cracking (EAC) in high-purity (HP) oxygenated water (0.4-9.0 ppm DO) at 289°C. K_{max} was increased in increments of ≈5 MPa·m$^{1/2}$ from the initial values of 5 and 10 MPa·m$^{1/2}$ at load ratios (R) of 0.2 and 0.6, respectively. The CGRs were compared with predicted results for wrought SSs in air in Section XI of the ASME Code and in oxygenated water from an Argonne National Laboratory (ANL) model reported in NUREG/CR-6176, ANL-94/1. The present and previous results were used to determine the dependence of K_{th}^{EAC} and ΔK_{th}^{EAC}, where $\Delta K_{th}^{EAC} = K_{th}^{EAC}(1 - R)$, on load ratio for specimens of Types 347, 316NG, and sensitized 304 SS, and thermally aged CF-3 and CF-8 grades of cast SS. Regimes where CGRs in water follow either the "air-line" at K_{max} and ΔK values below the threshold for EAC or model predictions in water at higher stress intensity factors were delineated. At K_{max} values <20 MPa·m$^{1/2}$, where EAC in not significant, CGRs lie below predictions of the ANL model in water by factors of ≈10 and 100 at load ratios of 0.6 and 0.95, respectively. Based on the present results, it

may be more appropriate to utilize the "air line" when assessing crack growth of these steels in water for K_{max} values below ≈20 MPa·m$^{1/2}$.

Metallographic evaluation of the specimens after the experiments indicated that the mode of cracking in the wrought and cast specimens was transgranular at load ratios ≤0.6, and that the crack path in the cast SS specimens traversed the austenite grains in these tests, in contrast with previous tests at a load ratio of 0.95, in which the crack path preferred the ferrite/austenite phase boundaries in the cast materials.

Irradiation-Assisted Stress Corrosion Cracking of Type 304 SS

Although significant grain-boundary chromium depletion can play an important role in irradiation-assisted stress corrosion cracking (IASCC) of thermally sensitized and irradiated components, we suspect that another primary process that involves trace impurity elements, which are not specified in the ASTM specifications, may contribute to IASCC of solution-annealed materials. Slow strain rate tensile test results on high- and commercial-purity Type 304 SS specimens irradiated to ≈2 x 10^{21} n·cm^{-2} (E >1 MeV) in several BWRs indicate that susceptibility to intergranular stress corrosion cracking (IGSCC) of the materials could be best explained on the basis of a combined role of fluorine and grain-boundary depletion of chromium. In this reporting period, more detailed analyses of fluorine have been conducted on ductile and intergranular fracture surfaces and on precipitates that were revealed by in-situ fracture of Type 304 and 348 SS specimens in the ultrahigh-vacuum environment of a scanning Auger microscope. Irradiated specimens from Type 304 SS heats that were more susceptible to IGSCC contained a higher level of fluorine than less susceptible heats. Fluorine content was higher in sulfide precipitates than in either carbide precipitates or the grain matrices, indicating that fluorine is trapped by the former type of precipitates. Trace levels of fluorine in SSs emerge when fluorspar, a neutral flux composed of ≈75% CaF_2, is used in the production of iron and steel. Fluorine contamination can also occur from weld slag and welding fumes during fabrication of large components when electrodes in submerged-arc and shielded-metal-arc welding are coated a with fluorine-containing flux. In addition, tubular products, such as neutron-absorber-rod tubes, are cleaned with pickling solutions that contain hydrofluoric acid.

Acknowledgments

The authors are grateful to Drs. Lee James and Dave Jones of Bettis Atomic Power Laboratory for providing the A302-Gr B steel, to Drs. F. Garzarolli and P. Dewes of Siemens Aktiengesellschaft, Erlangen, Germany, and to Dr. L. Nelson of Electric Power Research Institute, Palo Alto, California, for making available the irradiated Type 348 SS specimens. The authors thank W. F. Burke, J. C. Tezak, T. M. Galvin, and P. L. Torres for their contributions to the experimental effort. This work is sponsored by the Office of Nuclear Regulatory Research, U.S. Nuclear Regulatory Commission, under FIN Number A2212; Program Manager: Dr. M. B. McNeil.

1 Introduction

Fatigue and environmentally assisted cracking (EAC) of piping, pressure vessels, and core components in light water reactors (LWRs) are important concerns in operating plants and for extended reactor lifetimes. The degradation processes in U.S. reactors include fatigue of austenitic stainless steel (SS) in emergency core cooling systems* and pressurizer surge line** piping in pressurized water reactors (PWRs), intergranular stress corrosion cracking (IGSCC) of austenitic SS piping in boiling water reactors (BWRs), and propagation of fatigue or stress corrosion cracks (which initiate in sensitized SS cladding) in low-alloy ferritic steels in BWR pressure vessels.*** Similar cracking has also occurred in upper-shell-to-transition-cone girth welds in PWR steam generator vessels,+ and cracks have been found in steam generator feedwater distribution piping.++ Occurrences of mechanical-vibration-and thermal-fluctuation-induced fatigue failures in LWR plants in Japan have also been documented.[1]

Another concern is failure of reactor-core internal components after accumulation of relatively high fluence.+++ The general pattern of the observed failures indicates that, as nuclear plants age and neutron fluence increases, many apparently nonsensitized austenitic materials become susceptible to intergranular failure by a degradation process commonly known as irradiation-assisted stress corrosion cracking (IASCC). Some of these failures have been reported for components subjected to relatively low or negligible stress levels, e.g., control-blade sheaths and handles and instrument dry tubes of BWRs. Although most failed components can be replaced, some safety-significant structural components, such as the BWR top guide, shroud, and core plate, would be very difficult or impractical to replace. Research during the past six months has focused on fatigue of ferritic steels used in piping, steam generators, and pressure vessels; EAC of wrought and cast austenitic SSs and Alloy 600; and IASCC in high- and commercial-purity (HP and CP) Type 304 SS specimens from control-blade absorber tubes and a control-blade sheath used in operating BWRs.

2 Fatigue of Ferritic Steels

Plain carbon and low-alloy steels are used extensively in PWR and BWR steam supply systems as piping and pressure-vessel materials. The steels of interest in these applications include A106-Gr B and A333-Gr 6 for seamless pipe and A302-Gr B, A508-2, and A533-Gr B plate for pressure vessels. The ASME Boiler and Pressure Vessel Code Section III,[2] Subsection NB, which contains rules for the construction of Class 1 components for nuclear power plant, recognizes fatigue as a possible mode of failure in pressure vessel steels and piping materials. Figure I-90 of Appendix I to Section III of the

* USNRC Information Notice No. 88-08, "Thermal Stresses in Piping Connected to Reactor Coolant Systems," June 22, 1988; Supplement 1, June 24, 1988; Supplement 2, August 4, 1988; Supplement 3, April 11, 1989.

** USNRC Information Notice No. 88-11, "Pressurizer Surge Line Thermal Stratification," December 20, 1988.

*** USNRC Information Notice No. 90-29, "Cracking of Cladding in Its Heat-Affected Zone in the Base Metal of a Reactor Vessel Head," April 30, 1990.

+ USNRC Information Notice No. 90-04, "Cracking of the Upper Shell-to-Transition Cone Girth Welds in Steam Generators," January, 26, 1990.

++ USNRC Information Notice No. 91-19, "Steam Generator Feedwater Distribution Piping Damage," March 12, 1991.

+++ USNRC Information Notice No. 93-79, "Core Shroud Cracking at Beltline Region Welds in Boiling-Water Reactors," September 1993.

ASME Code specifies the fatigue design curves for the applicable structural materials. However, Section III, Subsection NB-3121 of the Code states that environmental effects on fatigue resistance of the material are not explicitly addressed in these design fatigue curves. Therefore, effects of environment on fatigue resistance of materials in all operating PWR and BWR plants whose primary coolant pressure boundary components are constructed to the specification of Section III of the Code are somewhat uncertain.

The current Code design curves are based primarily on strain-controlled fatigue tests of small polished specimens in air at room temperature.[3] To obtain the Code fatigue design curves, best-fit curves to the experimental data were decreased by a factor of 2 on stress or a factor of 20 on cycles, whichever was more conservative at each point. The factors were intended to account for uncertainties in translating experimental data of laboratory test specimens to actual reactor components. The factor of 20 on cycles is the product of three subfactors: 2.0 for scatter of data (minimum to mean), 2.5 for size effects, and 4.0 for surface finish, atmosphere, etc.[4] "Atmosphere" was intended to reflect the effects of an industrial environment rather than the controlled environment of a laboratory. The effects of the coolant environment are not explicitly addressed in the Code design curves.

Recent fatigue strain vs. life (S-N) data from the U.S.[5-15] and Japan[16-18] illustrate potentially significant effects of LWR environments on the fatigue resistance of carbon and low-alloy steels. In some cases, failures were observed below the ASME Code fatigue design curve. These results raise the issue of whether the fatigue design curves in Section III are appropriate for the purposes intended and whether they adequately account for effects of environment on fatigue behavior. The factors of 2 and 20 applied to the mean-data curve may not be as conservative as originally intended.

The primary sources of relevant data on fatigue of ferritic steel in LWR environments are the data obtained by General Electric Co. (GE) in a test loop at the Dresden 1 reactor,[5,6] tests performed by GE/Electric Power Research Institute (EPRI),[7,8] the work of Terrell at Materials Engineering Associates (MEA),[9-11] the present work at Argonne National Laboratory (ANL),[12-15] and the JNUFAD* data base for "Fatigue Strength of Nuclear Plant Components" from Japan, including the published work for A508-Cl 3 low-alloy steel and A333-Gr 6 carbon steel by Higuchi and Iida[16] and Iida et al.[17] and for forged A508-Cl 3 and rolled A533-Gr B low-alloy steels by Nagata et al.[18] The results show that, although the structure and cyclic-hardening behavior of carbon and low-alloy steels are distinctly different, there is little or no difference in susceptibility to environmental degradation of fatigue life of these steels when sulfur levels are comparable.[14,15] The A106-Gr B carbon steel exhibits pronounced dynamic strain aging, whereas strain aging effects are modest in A533-Gr B low-alloy steel.

The data indicate that water can have a significant effect on fatigue life only when all of the following four conditions are satisfied: sulfur content of the steel is >0.003 wt.%, temperature of the water is ≥150°C, concentration of dissolved oxygen (DO) in the water is ≥0.05 ppm, and applied strain rate is ≤1%/s. Although these are minimum conditions

* Private communication from M. Higuchi, Ishikawajima-Harima Heavy Industries Co., Japan, to M. Prager of the Pressure Vessel Research Council (PVRC), January 1992. The old database "FADAL" has been revised and renamed "JNUFAD."

that must be met to produce significant degradation in fatigue life, the actual dependence of fatigue life on these variables involves complex synergistic interactions. When any one of the four threshold conditions is not satisfied, e.g., at very low DO levels, which are characteristic of PWRs and BWRs with hydrogen–water chemistry, or at temperatures <150°C, environmental effects on fatigue life are modest.

For both carbon and low–alloy steel, the results indicate only a marginal effect of simulated PWR water on fatigue life, e.g., fatigue life is lower in PWR water than in air by less than a factor of 2. Furthermore, fatigue life is independent of strain rate; a three orders of magnitude decrease in strain rate does not cause an additional decrease in life.[15]

Effects of environment on fatigue life are significant at high DO levels, e.g., ≥0.5 ppm DO. The fatigue life of carbon and low–alloy steels decreases rapidly with decreasing strain rate. For both steels, the effect of strain rate saturates at ≈0.001%/s. Compared with tests in air, fatigue life of A106–Gr B steel in high DO water is lower by factors of 2, 4, 10, and 18 at strain rates of 0.4, 0.04, 0.004, and 0.0004%/s, respectively. A further decrease in strain rate by an order of magnitude does not cause an additional decrease in life. Furthermore, a minimum amount of strain is required for environmentally assisted degradation of fatigue life. For the heats of carbon and low–alloy steels that we investigated, this threshold strain range appears to be at ≈0.36%. The results also indicate that a slow strain rate applied during the tensile–loading cycle is more effective in environmentally assisted reduction of fatigue life than a slow strain rate applied during the compressive–loading cycle. Also, a slow strain rate applied during a compressive– as well as a tensile–loading cycle does not cause further decrease in fatigue life.

A detailed metallographic examination of the test specimens and several exploratory tests indicate that the reduction in fatigue life in high–DO water is primarily due to environmental effects on fatigue crack propagation. Environment appears to have little or no effect on crack nucleation. Although all specimens tested in water show surface micropitting, there is no indication that these micropits enhance crack nucleation. Irrespective of environment, cracks in carbon and low–alloy steels nucleate either along slip bands, carbide particles, or at ferrite/pearlite phase boundaries.

Based on existing fatigue S–N data, researchers at ANL have developed interim fatigue design curves that take into account temperature, DO concentration in water, sulfur level in steel, and strain rate.[19] A statistical model has also been developed for estimating the effects of various material and loading conditions on fatigue life of carbon and low–alloy steels.[20] Results of the statistical analysis have been used to estimate the probability of initiating fatigue cracks.

2.1 Technical Progress (O. K. Chopra, W. F. Michaud, and W. J. Shack)

The objectives of our task are to conduct fatigue tests on carbon and low–alloy steels under conditions where information is lacking in the existing S–N data base, establish the effects of material and loading variables on environmentally assisted reduction of fatigue life, and validate and update the proposed interim fatigue design curves. Fatigue tests are being conducted on A106–Gr B carbon and A533–Gr B low–alloy steel in water and in air at 288°C. During the present reporting period, fatigue tests have been conducted on

A302–Gr B low–alloy steel to verify whether the current predictions of modest decreases of fatigue life in simulated PWR water are valid for high–sulfur heats that show environmentally enhanced fatigue crack growth rates (CGRs) in precracked specimens. The effect of hold periods at peak tensile strain on the fatigue life of A106–Gr B carbon steel was also investigated.

2.1.1 Experimental

Low–cycle fatigue tests are being conducted on A106–Gr B carbon steel and A533–Gr B and A302–Gr B low–alloy steels with MTS closed–loop electrohydraulics machines. The A106–Gr B material was obtained from a 508–mm–diameter, schedule 140 pipe fabricated by the Cameron Iron Works, Houston, TX. The A533–Gr B material was obtained from the lower head of the Midland reactor vessel, which was scrapped before the plant was completed. The A302–Gr B low–alloy steel had been used in a previous study of the effect of temperature and cyclic frequency on fatigue crack growth behavior in a high–temperature aqueous environment at the Bettis Atomic Power Laboratory.[21] The material showed increased CGRs in simulated PWR water at 243°C. The chemical compositions and heat treatments of the materials are given in Table 1. The main difference between the steels is the sulfur content; i.e., 0.025% S for A302–Gr B and ≈0.015% S for A533–Gr B steel. Microstructures of the A302–Gr B steel along three orientations, i.e., rolling, transverse, and radial,* are shown in Fig. 1. The structure primarily consists of tempered ferrite plus bainite. However, the morphology of sulfides in the three orientations differs significantly.

Table 1. Chemical composition of ferritic steels for fatigue tests

Material	Source/ Reference[a]	Chemical Composition								
		C	P	S	Si	Fe	Cr	Ni	Mn	Mo
					Carbon Steel					
A106–Gr B[a]	ANL	0.29	0.013	0.015	0.25	Bal	0.19	0.09	0.88	0.05
	Supplier	0.29	0.016	0.015	0.24	Bal			0.93	
A106–Gr B	Terrell	0.26	0.008	0.020	0.28	Bal	0.015	0.002	0.92	0.003
A333–Gr 6	Higuchi	0.20	0.020	0.015	0.31	Bal	–	–	0.93	–
					Low–Alloy Steel					
A533–Gr B[b]	ANL	0.22	0.010	0.012	0.19	Bal	0.18	0.51	1.30	0.48
	Supplier	0.20	0.014	0.016	0.17	Bal	0.19	0.50	1.28	0.47
A533–Gr B	JNUFAD	0.19	0.020	0.010	0.27	Bal	0.13	0.60	1.45	0.52
A302–Gr B[c]	Bettis	0.19	0.026	0.024	0.22	Bal	0.14	0.23	1.29	0.55
	Supplier	0.19	0.015	0.027	0.21	Bal	–	–	1.17	0.48

[a]508–mm schedule 140 pipe fabricated by Cameron Iron Works, Heat J–7201. Actual heat treatment not known.

[b]162–mm thick hot–pressed plate from Midland reactor lower head. Austenitized at 871–899°C for 5.5 h, brine quenched and tempered at 649–663°C for 5.5 h, and brine quenched. The plate was machined to a final thickness of 127 mm. The surface was inlayed with 4.8–mm weld cladding and stress relieved at 607°C for 23.8 h.

[c]102–mm thick plate. Austenitized at 899–927°C for 4 h, water quenched to 538°C, and air cooled; tempered at 649–677°C; then stress relieved at 621–649°C for 6 h (up to 6 cycles).

* The three orientations are represented by the direction that is perpendicular to the plane of the photomicrograph.

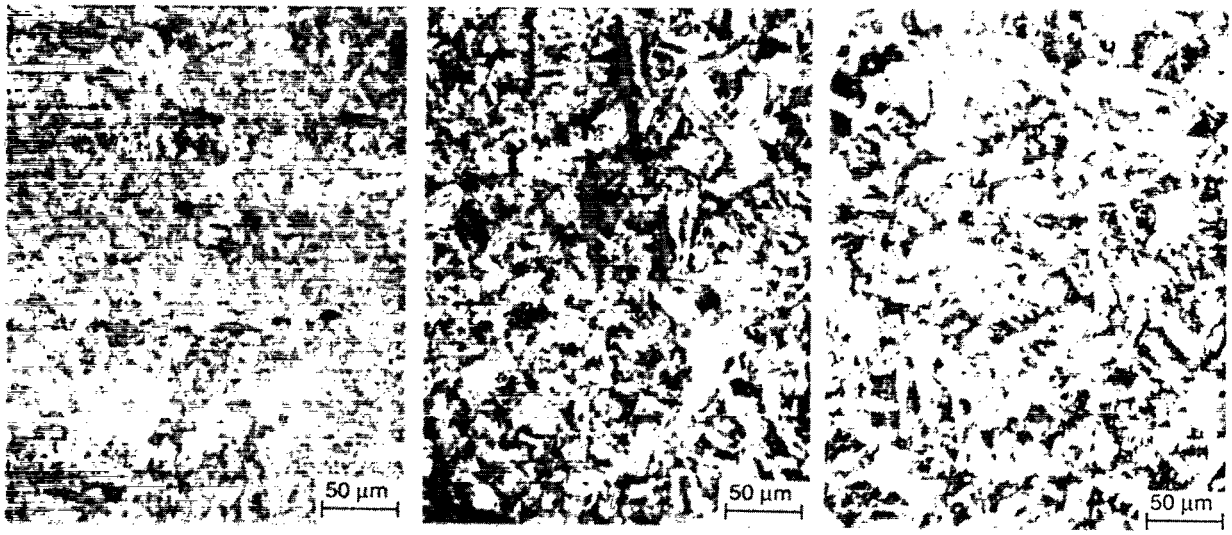

(a) (b) (c)

Figure 1. Microstructures along fracture planes of A302–Gr B steel specimens with orientations in (a) rolling, (b) transverse, and (c) radial directions. Plane of photomicrographs is represented by direction perpendicular to the plane.

Smooth cylindrical specimens with 9.5–mm diameter and 19–mm gage length were used for the fatigue tests. The test specimens of A302–Gr B steel were machined from a composite bar fabricated by electron–beam welding from two 19.8–mm diameter, 137–mm long bars of A533–Gr B steel on each side of an 18.8–mm diameter, 56–mm long section of A302–Gr B steel, Fig. 2. Thus, the gage length and shoulders of the specimen were A302–Gr B and the grip region was A533–Gr B steel. The A302–Gr B gage section of the specimens was oriented along the rolling direction. After welding, the composite bar was stress relieved at 650°C for 6 h.

All tests were conducted at 288°C, with fully reversed axial loading (i.e., load ratio R = –1) and a triangular or sawtooth wave form. Unless otherwise mentioned, the strain

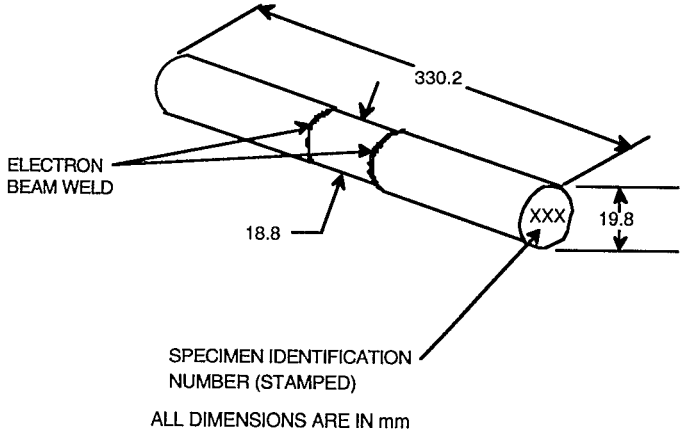

Figure 2. Schematic representation of electron–beam–welded bar used to fabricate A302–Gr B fatigue specimens

rate for the triangular wave and the fast-loading half of the sawtooth wave was 0.4%/s. Tests in water were performed under stroke control, where the specimen strain was controlled between two locations outside the autoclave. Tests in air were performed under strain control with an axial extensometer; specimen strain between the two locations used in the water tests was also recorded. Information from the air tests was used to determine the stroke required to maintain constant strain in the specimen gage length for tests in water; stroke was increased gradually during the test to maintain constant strain in the specimen. Detailed descriptions of the test facility and procedure have been presented earlier.[14]

2.1.2 A302-Gr B Steel

Fatigue tests were conducted in air and simulated PWR water, i.e., water containing <0.01 ppm DO, 2 ppm lithium, and 1000 ppm boron, at 288°C and a strain range of ≈0.75% with triangular and sawtooth wave forms. The fatigue results on A302-Gr B steel are summarized in Table 2. The various loading wave forms and corresponding fatigue data are presented in Fig. 3. The fatigue lives for A302-Gr B steel are compared with the fatigue S-N data for A533-Gr B steel in air and simulated PWR environments in Figs. 4 and 5, respectively.

Table 2. Fatigue test results for A302-Gr B low-alloy steel

Test Number	Environment[a]	Dissolved Oxygen, ppb	pH at RT	Conductivity, µS/cm	Tensile Rate, %/s	Comp. Rate, %/s	Stress Range, MPa	Strain Range, %	Life N_{25}, Cycles
1697	Air	–	–	–	0.4	0.4	944.5	0.756	8,070
1701	Air	–	–	–	0.004	0.4	1021.4	0.757	4,936
1712	Air	–	–	–	0.0004[b]	0.4	1041.9	0.759	5,350
1702	PWR	3.0	6.5	20.00	0.4	0.4	921.2	0.735	6,212
1704	PWR	3.0	6.5	19.23	0.004	0.4	1022.6	0.745	3,860
1716	PWR	4.5	6.5	19.23	0.0004[b]	0.4	1042.3	0.739	3,718

[a] Simulated PWR water contains 2 ppm lithium and 1000 ppm boron.
[b] Slow strain rate applied only during 1/8 cycle near peak tensile strain.

In both environments, the results for A302-Gr B steel are in good agreement with the data for A533-Gr B steel. The results indicate only a marginal effect of PWR water on fatigue life. The fatigue life of A302-Gr B steel is lower by ≈23% in PWR water than in air at both strain rates. Even the 1/8-cycle slow/fast test, with a slow strain rate of 0.0004%/s, shows only a moderate decrease in fatigue life. These results are consistent with data obtained earlier for A106-Gr B carbon steel and A533-Gr B low-alloy steel. The data suggest that even high-sulfur steels suffer only modest decreases of fatigue life in simulated PWR water. Additional fatigue specimens are being machined with the gage section orientation transverse to the rolling direction to establish possible effects of material orientation.

Although the steel is subject to only moderate environmental degradation of fatigue life, the results also indicate a significant effect of strain rate both in air and PWR water. Fatigue life decreases by ≈40% as strain rate decreases from 0.4 to 0.004%/s. This result is somewhat surprising because strain rate effects are not observed for other carbon or low-alloy steels in either air or simulated PWR water.

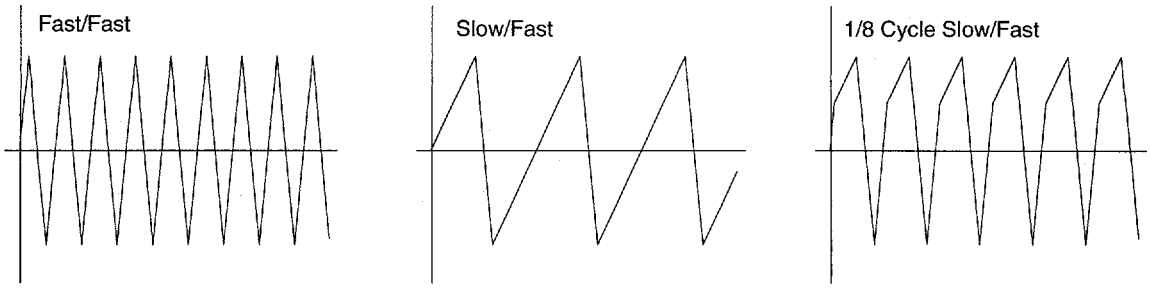

Strain rate: 0.4%/s in tension and compression		Strain rate: 0.004%/s in tension and 0.4%/s in comp.		Strain rate: 0.0004%/s during 1/8 cycle and 0.4%/s for remaining period	
Air:	8070 cycles	Air:	4936 cycles	Air:	5350 cycles
PWR:	6212 cycles	PWR:	3860 cycles	PWR:	3718 cycles

Figure 3. Fatigue life of A302–Gr B low–alloy steel at 288°C in air and simulated PWR water tested with triangular or sawtooth loading wave forms at a strain range of ≈0.75%

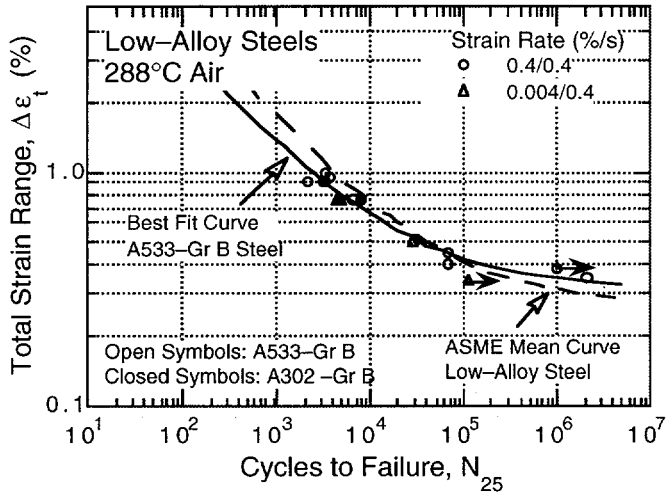

Figure 4.
Total strain range vs. fatigue life data for low–alloy steels in air

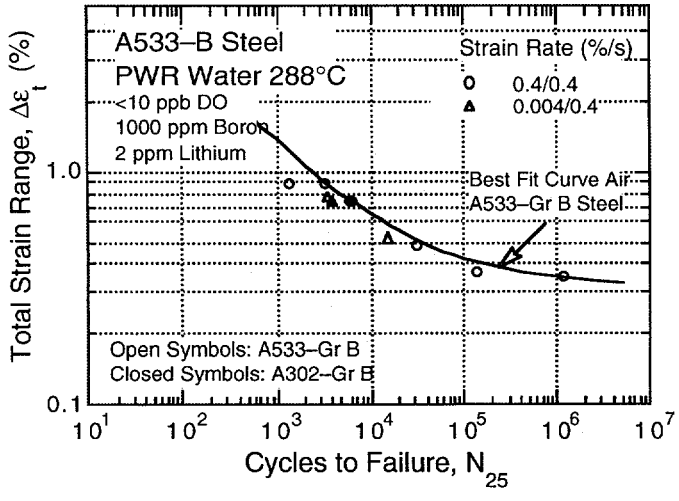

Figure 5.
Total strain range vs. fatigue life data for low–alloy steels in PWR water at 288°C

Figures 6 and 7 show the cyclic stress range vs. fatigue cycles for A302–Gr B and A533–Gr B low–alloy steels, respectively, in air at 288°C and a total strain range of ≈0.75%. Cyclic–hardening behavior of the steels is consistent with their microstructures. Both steels have a relatively high yield stress and moderate cyclic hardening occurs during the initial 100 cycles; A302–Gr B hardens more than A533–Gr B steel. The A302–Gr B steel exhibits some dynamic strain aging; the material strain hardens significantly at slow strain rates.

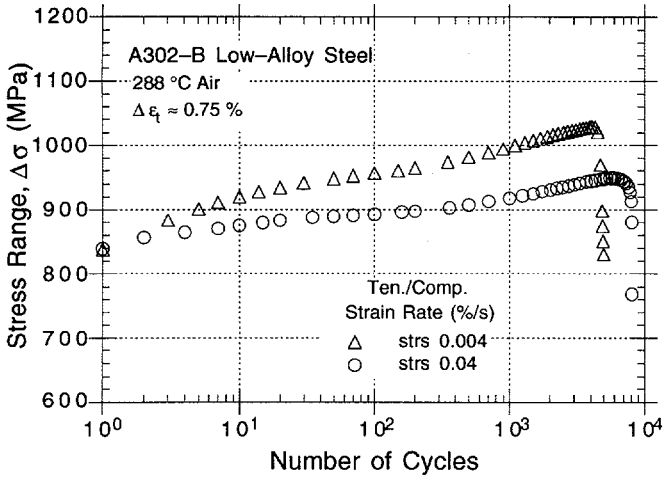

Figure 6.
Effect of strain rate on cyclic strain–hardening behavior of A302–Gr B steel in air at 288°C

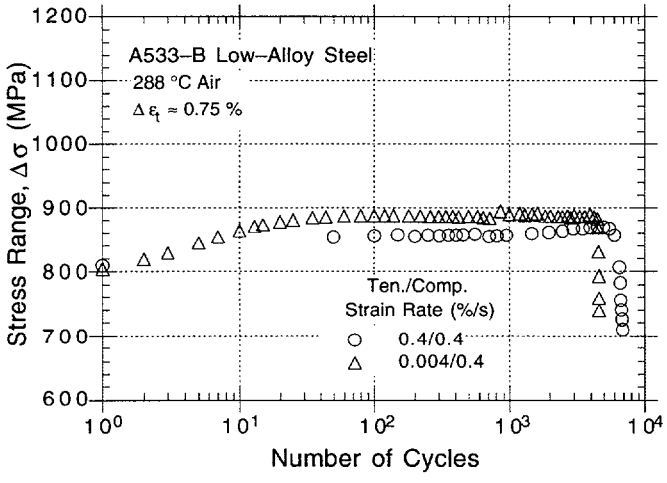

Figure 7.
Effect of strain rate on cyclic strain–hardening behavior of A533–Gr B steel in air at 288°C

Surface oxide films that develop on A302–Gr B steel specimens in air and simulated PWR water are essentially the same as those observed earlier for A106–Gr B carbon steel and A533–Gr B low–alloy steel.[14] Photomicrographs of the gage surface of A302–Gr B specimens tested in air and PWR water are shown in Fig. 8. The specimens tested in water developed a gray/black corrosion scale; X–ray diffraction analysis of the specimen surface indicated that the surface scale is primarily magnetite (Fe_3O_4). All specimens tested in water showed surface micropitting.

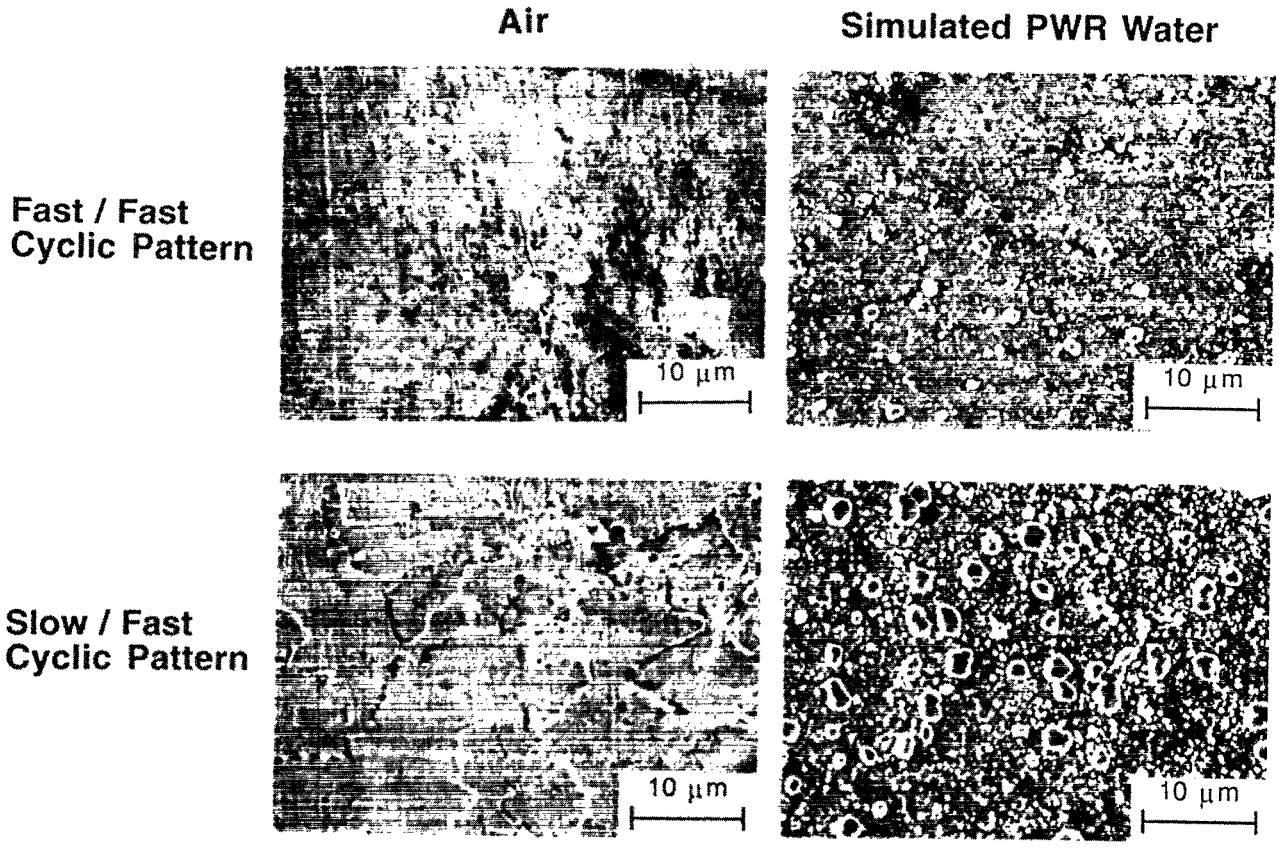

Figure 8. SEM photomicrographs of gage surface of A302–Gr B specimens tested in air and simulated PWR water at 288°C with triangular (top) and sawtooth (bottom) waveforms

2.1.3 Tensile Hold Periods

Tests were also conducted with a 5- or 30-min hold period at peak tensile strain. The loading wave forms, hysteresis loops, and fatigue lives for the tests are given in Fig. 9. The results indicate that a tensile hold period decreases fatigue life in high-DO water but not in air. A 5-min hold period is sufficient to reduce fatigue life; a longer hold period results in only a slightly larger decrease in life. Two 5-min hold-time tests at 288°C and a strain range of ≈0.8% in water with 0.7 ppm DO gave fatigue lives of 1007 and 1092 cycles. Fatigue life was 840 cycles in a 30-min hold time test.

The fatigue tests in water were conducted in a stroke-controlled mode, which is somewhat different from a conventional hold-time test in strain-controlled mode. In a strain-controlled test, the total strain in the sample is held constant during the hold period. However, a portion of the elastic strain is converted to plastic strain because of stress relaxation. In stroke-controlled tests, there is an additional plastic strain in the sample due to relaxation of elastic strain from the load train (Fig. 9). Consequently, these are not true constant-strain-hold periods but include significant strain during the hold period; the measured plastic strains during the hold period were ≈0.028% from relaxation of the gage and 0.05–0.06% from relaxation of load train. These conditions result in strain rates of 0.005–0.02%/s during the hold period.

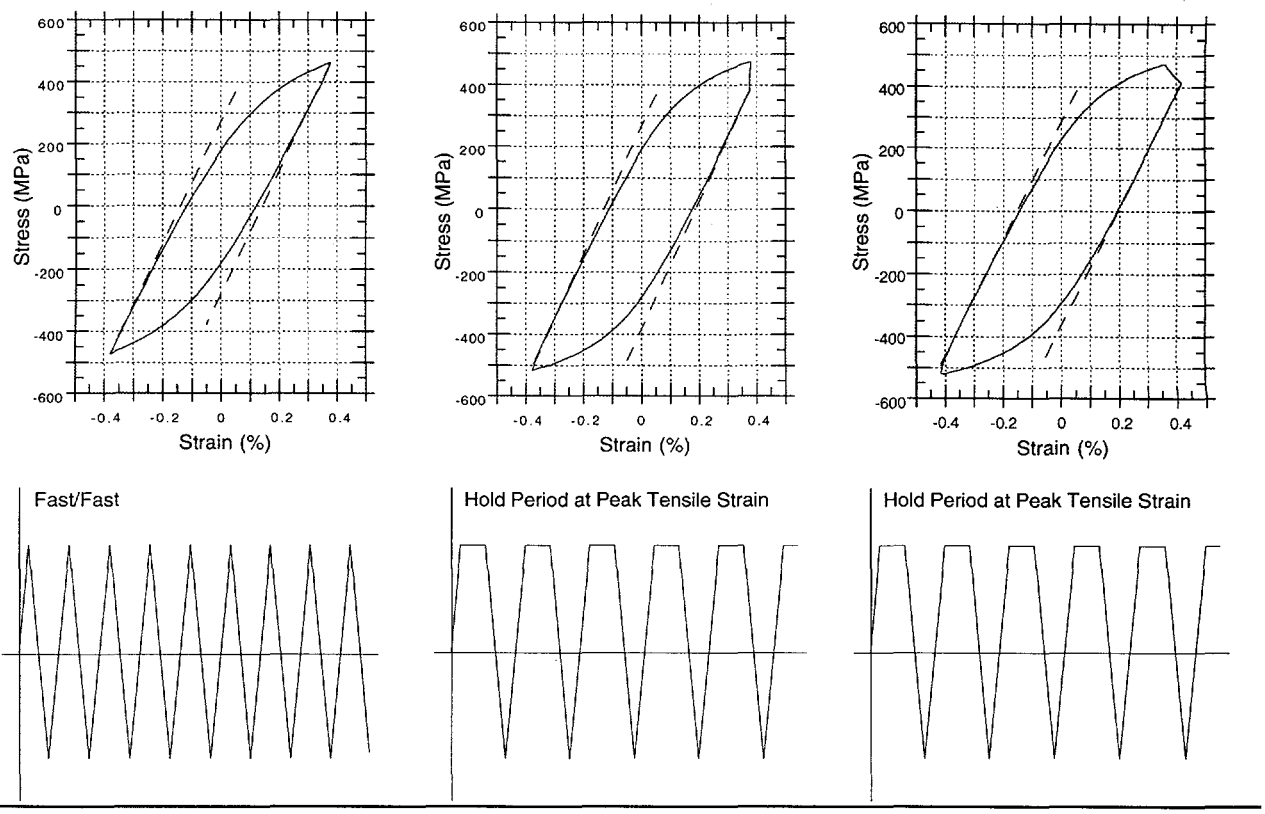

Strain or Stroke Control		Strain Control		Stroke Control (5–min hold)	
Air:	4740±1250 cycles	Air:	6,275 cycles	Air:	2592 cycles
PWR:	1965±385 cycles			High DO:	1007, 1092 cycles
High DO:	2077 cycles			Stroke Control (30–min hold)	
				High DO:	840 cycles

Figure 9. Fatigue life of A106–Gr B steel in air and water environments at 288°C, strain range of ≈0.75%, and hold periods at peak tensile strain. Hysteresis loops are for tests in air.

2.1.4 Conclusions

Fatigue tests have been conducted on A302–Gr B low–alloy steel to verify whether the current predictions of modest decreases of fatigue life in simulated PWR water are valid for high–sulfur heats that show environmentally enhanced fatigue CGRs in precracked specimens. This A302–Gr B low–alloy steel contains high sulfur (0.027 wt.%) and exhibits increased CGRs in simulated PWR water (<10 ppb DO). The results for A302–Gr B steel are consistent with data obtained earlier for A106–Gr B carbon steel and A533–Gr B low–alloy steel. The data suggest that even steels with very high sulfur suffer only modest decreases of fatigue life in simulated PWR water.

Tests have also been conducted on A106–Gr B carbon steel in high–DO water at 288°C, a strain range of ≈0.75%, and 5– or 30–min hold periods at peak tensile strain. The results indicate that a hold period at peak tensile strain decreases fatigue life in high–DO water but not in air. A 5–min hold period is sufficient to reduce fatigue life.

3 Environmentally Assisted Cracking of Wrought and Cast SSs in Simulated BWR Water

The objective of this work is to evaluate the resistance of wrought and cast austenitic SSs to EAC in simulated BWR water. Alternative materials for recirculation system piping in BWRs, e.g., Types 316NG and 347 SS, are very resistant to sensitization and thus are much less susceptible to IGSCC than Types 304 and 316 SS used in many operating reactors in the U.S. However, Type 316NG SS can undergo other modes of degradation, such as transgranular stress corrosion cracking and corrosion-assisted fatigue, in simulated reactor water chemistries.

Cast duplex SSs are used extensively in the nuclear industry in pump casings, valve bodies, piping, and other components in coolant systems of LWRs. The steels correspond to ASTM Specification A-351 grades CF-3, CF-3A, CF-8, CF-8A, and CF-8M, where the compositions of CF-3A and CF-8A fall within the composition limits of CF-3 and CF-8, but are further restricted to obtain ferrite/austenite ratios that result in higher ultimate and yield strengths. The molybdenum-free CF-3 and CF-8 grades contain low- and high-carbon concentrations (<0.03 and <0.08 wt.%, respectively) and are similar in composition to wrought Types 304L and 304 SS. The molybdenum-containing CF-3M and CF-8M grades with low- and high-carbon content are similar to Types 316L and 316 SS, respectively. After many years of service at reactor operating temperatures, these steels can undergo thermal aging embrittlement that is caused by precipitation and growth of a chromium-rich α' phase, an nickel- and silicon-rich G phase, $M_{23}C_6$, γ (austenite) in the ferrite, and additional precipitation and/or growth of existing carbides at the ferrite/austenite phase boundaries.[22-31] These compositional changes increase the tensile strength[32] and decrease the impact energy and fracture toughness of the steels.[33-43] In general, the low-carbon CF-3 grade is most resistant and the molybdenum-bearing high-carbon CF-8M grade is least resistant to thermal embrittlement.[33,36]

Cracking of cast SS components exposed to LWR coolants is rather infrequent compared with that of other materials. However, an inspection of the drywell of a BWR to determine the cause of an increase in unidentified leakage revealed a through-wall crack in the manual gate valve in the condensate return line of the emergency condenser system.* Subsequently, the internal components of other valves in the emergency condenser system were removed and inspected by visual, radiographic, and ultrasonic tests. Inspections of the inner surface of the valves revealed cracks near drain holes in the valve bodies, which were made from CF-8M SS. Some of the cracks were within 0.15-0.35 in. of passing through the 1.25-in. wall thickness (≈70-90% through wall). A metallographic examination of a boat specimen revealed that the material contained ≈15% delta ferrite and that the crack propagated transgranularly with little secondary cracking, which is characteristic of a fatigue crack.

The purpose of the present work is to determine the effect of load ratio R on the threshold stress intensity K_{th} for EAC of wrought and cast grades of austenitic SS in oxygenated high-temperature water. An abrupt transition in the magnitude of the CGRs

* NRC Information Notice 92-50: "Cracking of Valves in the Condensate Return Lines of a BWR Emergency Condenser System," July 2, 1992.

from the "air curve" predicted by the ASME Code Section XI correlation at low values of maximum stress intensity K_{max} to a water curve at higher values will be incorporated into the set of equations[44] for corrosion fatigue crack growth of austenitic SSs in aqueous environments.

3.1 Technical Progress (W. E. Ruther, W. K. Soppet, and T. F. Kassner)

During this reporting period, fracture-mechanics CGR tests were completed on 1T-compact tension (CT) specimens of Type 316NG and 304 SS and as-received and thermally aged CF-3 cast SS in oxygenated water at 289°C. The composition of Type 316NG, 304, and CF-3 SS specimens for CGR experiments are shown in Table 3, along with that of other steels used to investigate threshold stress intensity factors for EAC.

Table 3. Chemical composition of wrought and cast austenitic SSs for corrosion fatigue tests in oxygenated HP water

Grade	Heat No.	Composition, wt.%								
		C	N	P	S	Si	Ni	Cr	Mo	Mn
316NG	13198	0.013	0.085	0.022	0.017	0.64	10.70	16.51	2.08	1.63
316NG	D432804	0.015	0.109	0.023	0.002	0.52	12.75	17.48	2.40	1.70
316NG	P91576	0.015	0.068	0.020	0.010	0.42	10.95	16.42	2.14	1.63
304	30956	0.060	0.100	0.019	0.007	0.48	8.00	18.99	0.44	1.54
CF-8[a]	68	0.063	0.062	0.021	0.014	1.07	8.08	20.64	0.31	0.64
CF-3[a]	P2	0.019	0.040	0.019	0.006	0.94	9.38	20.20	0.16	0.74
CF-3[a]	69	0.023	0.028	0.015	0.005	1.13	8.59	20.18	0.34	0.63

[a] Measured ferrite content of cast SSs was 23.4% for CF-8, Heat No. 68; 15.6% for CF-3, Heat No. P2; and 23.6% for Heat No. 69.

3.1.1 Threshold Stress Intensity for EAC of Type 316NG and 304 SS

Six tests were performed on a set of three specimens from different heats of Type 316NG SS to measure the threshold stress intensity for SCC (K_{scc}) in HP water containing ≈6 ppm DO at 289°C. The test conditions and experimental results are shown in Table 4. The CGR results at a load ratio R of 0.6 and K_{max} values between 10 and 74 MPa·m$^{1/2}$ are shown in Figs. 10 and 11. K_{max} was increased in increments of ≈5 MPa·m$^{1/2}$ from the initial value of 10 MPa·m$^{1/2}$ to 20 MPa·m$^{1/2}$ at this R value as the experiment progressed. The arrows associated with data in Figs. 10 and 11 at CGRs of $<3 \times 10^{-11}$ m·s^{-1} denote that the rates are based on the sensitivity of the dc potential crack-length monitoring system, namely, 5×10^{-5} m divided by test times of ≈500 h. Deep cracks and high CGRs in the last phase of the experiment yielded stress intensity factors >40 MPa·m$^{1/2}$. The CGRs of the specimens were near or below the "air line" predicted by the ASME Section XI correlation at K_{max} values <25 MPa·m$^{1/2}$ and were consistent with ANL model predictions[44] for crack growth in water at higher K_{max} values (Fig. 11). The results in Fig. 11 suggest a threshold K_{max} for EAC of ≈26 MPa·m$^{1/2}$ at a load ratio of 0.6.

Table 4. Crack growth results for Type 316NG SS specimens[a] in HP oxygenated water at 289°C

		Water Chemistry [b]			Electrode Potential			Type 316NG SS					
								Heat 13198		Heat D432804		Heat P91576	
Test No.	Test Time, h	Cond. at 25°C, $\mu S \cdot cm^{-1}$	pH at 25°C	O_2, ppm	304 SS mV(SHE)	Pt mV(SHE)	Load Ratio[c]	K_{max}[d], MPa·$m^{1/2}$	Rate, 10^{-10} m·s^{-1}	K_{max}[d], MPa·$m^{1/2}$	Rate, 10^{-10} m·s^{-1}	K_{max}[d], MPa·$m^{1/2}$	Rate, 10^{-10} m·s^{-1}
1	385–985	0.08	6.32	4.4	105	162	0.20	5.0	<0.2[e]	5.0	0.2	5.0	<0.2[e]
2	1030–1502	0.09	6.32	6.2	125	175	0.60	10.0	<0.3[e]	10.1	<0.3[e]	10.0	<0.3[e]
3	1710–2100	0.10	6.38	5.6	122	158	0.60	15.0	<0.3[e]	15.2	<0.3[e]	15.0	<0.3[e]
4	2140–2354	0.09	6.28	6.0	123	158	0.60	20.9	11.3	20.3	0.4	21.0	13.0
5	2377–2477	0.09	6.15	6.0	122	152	0.60	30.2	76.3	26.0	13.4	30.9	83.3
6	2500–2590	0.09	6.12	6.2	121	154	0.60	73.8	317.0	37.7	128.0	64.9	282.0

[a] Compact tension specimens (1T–CT) of Type 316NG SS (Heat Nos. 13198, D432804, and P91576). The specimens (Nos. CTD–198–3, CTD–4–1, and CTD–9–8, respectively) received a solution–anneal heat treatment at 1050°C for 0.5 h plus a sensitization–type heat teatment at 650°C for 24h.

[b] Effluent dissolved–oxygen concentration was ≈4–6 ppm; feedwater oxygen concentration was slightly higher to compensate for oxygen depletion by corrosion of the autoclave system.

[c] Frequency and rise time of the positive sawtooth waveform were 7.7×10^{-2} Hz and 12 s, respectively.

[d] Stress intensity K_{max} values at the end of the time period.

[e] Value based on the sensivity of the crack length measurement (5×10^{-5} m) divided by the test time.

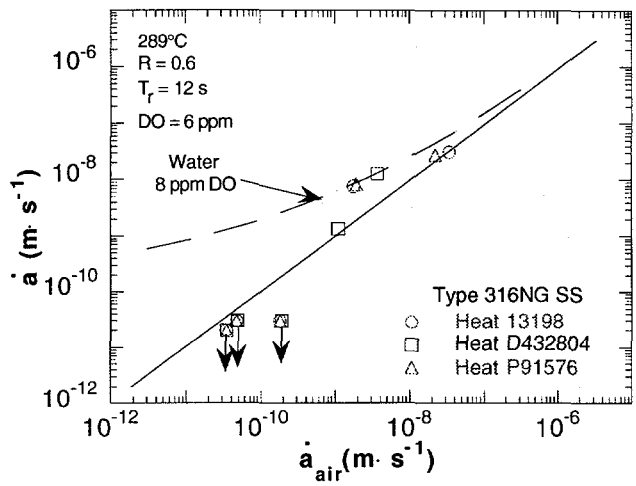

Figure 10.
Corrosion fatigue data for specimens from three heats of Type 316NG SS in HP oxygenated water at 289°C. Dashed line represents model predictions at an R value of 0.6 and rise time of 12 s in water containing 8 ppm DO. Solid line corresponds to crack growth of SSs in air.

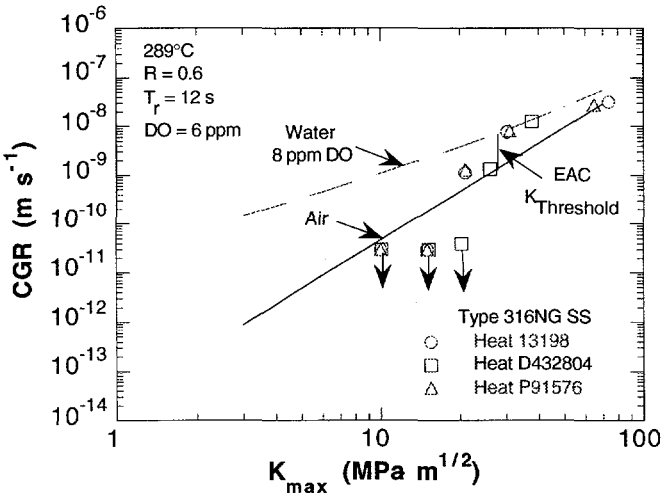

Figure 11.
Dependence of CGR of specimens from three heats of Type 316NG SS on K_{max} in HP oxygenated water at 289°C. Dashed and solid lines represent model predictions in water containing 8 ppm DO and in air, respectively, at R value of 0.6 and rise time of 12 s.

Analogous CGR tests were performed on a set of three specimens, namely, another heat of Type 316NG SS, lightly sensitized (EPR =2 C·cm^2) Type 304 SS, and thermally aged (30,000 h at 350°C) CF–3 SS at a load ratio of 0.2. The tests were conducted in HP water containing ≈7–9 ppm DO at 289°C at K_{max} values between 5 and 54 MPa·m$^{1/2}$. The results are shown in Table 5 and Figs. 12 and 13. Several data points for the Type 304 and CF–3 SS specimens lie below the air line predicted by the ASME Code at K_{max} values between ≈10 and 18 MPa·m$^{1/2}$. For the most part, the CGRs are consistent with Code predictions in air, i.e., environmental enhancement in the rates is small, although the results for Type 316NG, CF–3, and 304 SS specimens suggest threshold K_{max} values for EAC of ≈22, 25 and 27 MPa·m$^{1/2}$, respectively, at a load ratio of 0.2. The CGRs of both specimens lie somewhat above the air line at higher K_{max}; however, the predicted rates in air and water tend to converge at K_{max} values >30 MPa·m$^{1/2}$. Within the uncertainty of the measurements, the sensitized Type 304 SS specimen does not exhibit a clear threshold K_{max} for EAC in Fig 13.

Table 5. Crack growth results for Types 316NG, 304, and CF-3 cast SS 1T-CT specimens[a] under cyclic loading[b] in water at 289°C

Test No.	Time, h	Cond., μS·cm^{-1}	O_2,[c] ppm	Potentials 304 SS, mV(SHE)	Potentials Pt, mV(SHE)	Load Ratio	Freq., 10^{-2} Hz	Rise Time, s	316NG (No. CTP9-3) (EPR = 0 C·cm^{-2}) K_{max}[d], MPa·m$^{1/2}$	316NG (No. CTP9-3) (EPR = 0 C·cm^{-2}) Rate, 10^{-10} m·s^{-1}	304 Sensitized (No. 20) (EPR = 2 C·cm^{-2}) K_{max}[d], MPa·m$^{1/2}$	304 Sensitized (No. 20) (EPR = 2 C·cm^{-2}) Rate, 10^{-10} m·s^{-1}	CF-3 (No. P2T-12) Aged (30,000 h @ 350°C) K_{max}[d], MPa·m$^{1/2}$	CF-3 (No. P2T-12) Aged (30,000 h @ 350°C) Rate, 10^{-10} m·s^{-1}
1	110–550	0.075	7.2	252	293	0.20	7.7	12	5.0	0.49	5.0	0.29	5.0	0.65
2	560–1030	0.077	6.8	266	282	0.20	7.7	12	10.3	7.42	10.1	0.47	10.0	0.15
3	1030–1175	0.080	8.1	263	285	0.20	7.7	12	16.6	29.1	15.1	3.3	14.9	0.30
4	1190–1240	0.077	9.1	260	282	0.20	7.7	12	23.0	150.0	18.2	5.1	18.0	12.7
5	1265–1275	0.094	9.0	262	281	0.20	7.7	12	26.2	228.0	19.8	15.0	19.6	25.3
6	1285–1305	0.094	8.5	262	282	0.20	7.7	12	32.4	275.0	22.9	56.2	22.9	80.8
7	1310–1325	0.094	8.8	262	282	0.20	7.7	12	38.4	335.0	25.2	90.3	25.6	142.0
8	1336–1347	0.094	8.8	262	282	0.20	7.7	12	42.6	340.0	26.7	115.0	27.4	161.0
9	1525–1545	0.091	7.6	257	291	0.20	7.7	12	Specimen	Removed	29.6	228.0	31.6	273.0
10	1550–1565	0.091	8.1	265	288	0.20	7.7	12	–	–	40.4	354.0	43.8	377.0
11	1575–1586	0.091	7.8	267	287	0.20	7.7	12	–	–	50.3	764.0	53.8	461.0

[a]Types 316NG (Heat No. 91576, Specimen No. CTP9-3), 304 (Heat No. 30956; Specimen No. 20), and cast CF-3 (Heat No. P2 containing 15.6% ferrite, Specimen No. P2T-12) SS. The specimens received the following heat treatments: Type 316NG SS, solution anneal at 1050°C for 0.5 h plus 650°C for 24 h (EPR = 0 C·cm^{-2}); Type 304 SS, solution anneal at 1050°C for 0.5 h followed by 700°C for 0.25 h plus 500°C for 24 h (EPR = 2 C·cm^{-2}); and cast CF-3 SS, 350°C for 30,000 h in air.

[b]Positive sawtooth wave form was used.

[c]Effluent dissolved-oxygen concentrations.

[d]Stress intensity K_{max} values at the end of the time period.

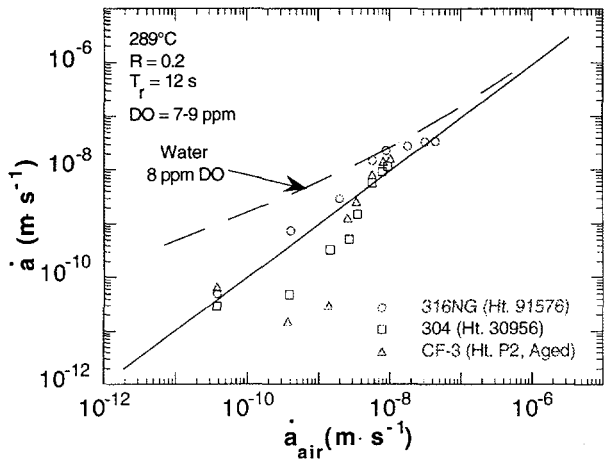

Figure 12.
Corrosion fatigue data for specimens of Type 316NG, sensitized Type 304, and thermally aged CF–3 SS in oxygenated water at 289°C. Dashed line represents ANL model predictions for austenitic SSs in water containing 8 ppm DO. Solid line corresponds to crack growth of SSs in air.

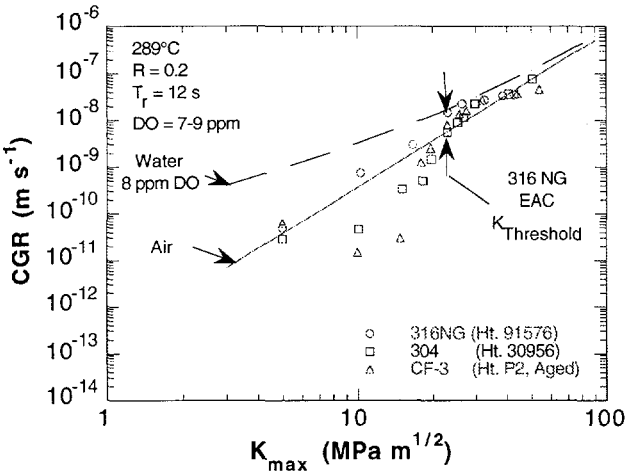

Figure 13.
Dependence of CGRs of Type 316NG, sensitized Type 304, and thermally aged CF–3 SS specimens on K_{max} in oxygenated water at 289°C. Dashed and solid lines represent model predictions for austenitic SSs in water containing 8 ppm DO and in air, respectively, at an R value of 0.2 and rise time of 12 s.

3.1.2 Threshold Stress Intensity for EAC of CF–3 and –8 Grades of Cast SS

Crack growth results for as–received and thermally aged specimens of cast SSs in fracture–mechanics tests in high–temperature water were presented in several previous reports.[45–47] The tests were conducted to characterize the effects of material composition, long–term thermal aging of the steels (30,000 h at 350°C), DO concentration in HP water, and loading conditions (namely, load ratio and stress intensity factor) on CGRs at 289°C. Several tests were conducted on as–received and thermally aged CF–8M SS in air at 289°C to provide baseline information for comparison with results for wrought SSs in air in Section XI of the ASME Code and in oxygenated water. The results, which indicated that long–term thermal aging had no effect on the CGRs of CF–8M SS in air, were consistent with predictions from the ASME Code at rates ≥5 x 10^{-10} m·s^{-1} but were below Code predictions by one order of magnitude at lower rates.[46] For the most part, the rates in water were bounded by the air curve from the Code and ANL correlations[44] for wrought SSs in water at 289°C. At stress intensity factors ≤30 MPa·m$^{1/2}$ and load ratios ≥0.90, which yield CGRs of <5 x 10^{-10} m·s^{-1} in water, the data were considerably below model predictions for crack growth in water containing 0.2 or 8 ppm DO.[47] This observation suggests that there is a threshold stress intensity for EAC of these steels that

may depend on load ratio as well as on alloy composition, heat treatment, and environment (i.e., DO level). This has been explored in subsequent tests and the results are described below.

A fracture-mechanics CGR experiment was conducted on specimens of CF-3 grade of cast SS in as-received and thermally aged (30,000 h at 350°C) conditions in HP water containing 0.4 ppm DO at 289°C. Six tests were performed on this set of specimens to measure the threshold K_{max} at a load ratio R of 0.6. K_{max} was increased in increments of ≈5 MPa·m$^{1/2}$ from the initial value of 15 MPa·m$^{1/2}$ to ≈57 MPa·m$^{1/2}$ as the experiment progressed. The results are shown in Table 6 and Figs. 14 and 15. High CGRs occurred in the last phases of the experiment at stress intensity factors >30 MPa·m$^{1/2}$. In Fig. 14, the CGR data are plotted versus calculated CGRs of wrought SSs in air under identical loading conditions. The data for the as–received specimen (Heat 69) are consistent with values predicted by the ASME Section XI correlation for crack growth in wrought SSs in air, whereas the results for the thermally aged specimens (Heats P2 and 69) lie below the "air line" at K_{max} values of <25 MPa·m$^{1/2}$, but show a similar dependence on K_{max}, and are somewhat above the air line at higher K_{max} values. The plot of the CGRs versus K_{max} in Fig. 15 shows an abrupt increase in the rates for the thermally aged specimens at a K_{max} of ≈25 MPa·m$^{1/2}$, which suggests an EAC threshold for these specimens. The CGRs for the as–received specimen follow the "air line" over the entire range of K_{max} values. At K_{max} and CGR values >30 MPa·m$^{1/2}$ and >1 x 10^{-8} m·s^{-1}, respectively, the curves corresponding to crack growth in water and air tend to merge, so it is difficult to establish whether a threshold stress intensity for EAC occurs in this range at a load ratio of 0.6.

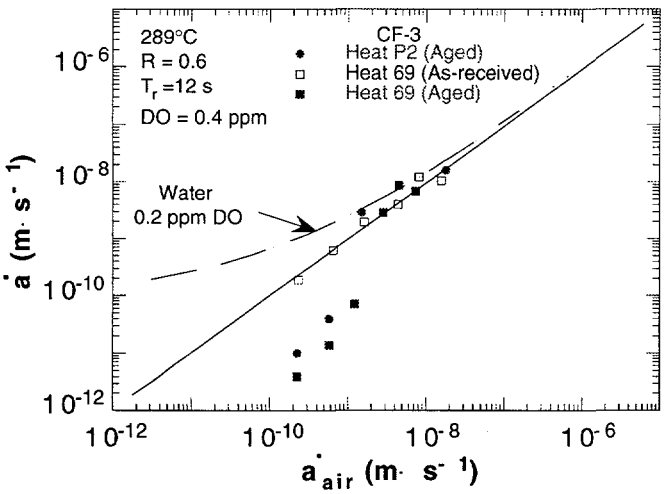

Figure 14. Corrosion fatigue data for as–received and thermally aged CF–3 SS in HP oxygenated water at 289°C. Dashed line represents model predictions at an R value of 0.6 and rise time of 12 s in water containing 0.2 ppm DO. Solid line corresponds to crack growth of wrought SSs in air.

Results reported previously[47] for thermally aged CF–8 SS in oxygenated water at a load ratio of 0.95 (Fig. 16) indicate a threshold K_{max} for EAC of ≈37 MPa·m$^{1/2}$. The data in Figs. 13, 15, and 16 indicate the threshold stress intensity for EAC of the thermally aged cast SSs, i.e., a transition from the air curve (or below) at lower values of K_{max} to a water curve at higher values, decreases as the load ratio decreases. However, as the load ratio decreases, e.g., from 0.95 to 0.2, the degree of environmental enhancement of the CGRs relative to that in air also decreases, as can be seen in these figures. The data are consistent with model predictions for wrought SSs, which show that as the load ratio

Table 6. Crack growth results for CF–3 cast SS specimens[a] under cyclic loading[b] in HP oxygenated water at 289°C

Test No.	Time, h	Cond., μS·cm^{-1}	O_2,[c] ppm	Potentials 304 SS, mV(SHE)	Potentials Pt, mV(SHE)	Load Ratio	Freq., 10^{-2} Hz	Rise Time, s	CF–3 (No. P2T–11) Aged (30,000 h @ 350°C) K_{max}[d], MPa·m$^{1/2}$	CF–3 (No. P2T–11) Aged (30,000 h @ 350°C) Rate, 10^{-10} m·s^{-1}	CF–3 (No. 692–08B) As–received K_{max}[d], MPa·m$^{1/2}$	CF–3 (No. 692–08B) As–received Rate, 10^{-10} m·s^{-1}	CF–3 (No. 692–03B) Aged (30,000 h @ 350°C) K_{max}[d], MPa·m$^{1/2}$	CF–3 (No. 692–03B) Aged (30,000 h @ 350°C) Rate, 10^{-10} m·s^{-1}
1	18 443	0.08	0.41	105	107	0.60	7.7	12	15.1	0.1	15.3	1.9	15.1	0.04
2	450 685	0.09	0.39	50	54	0.60	7.7	12	20.1	0.4	20.9	6.3	20.1	0.14
3	697 800	0.08	0.41	53	52	0.60	7.7	12	26.8	29.5	27.4	19.5	25.2	0.72
4	814 952	0.09	0.38	52	56	0.60	7.7	12	56.8	160.0	37.2	39.8	32.5	28.6
5	1221 1263	0.07	0.45	4	14	0.60	7.7	12	Specimen	Removed	44.7	122.7	37.5	87.7
6	1269 1317	0.07	0.40	–25	15	0.60	7.7	12	–	–	54.7	105.9	43.5	68.8

[a]Compact tension specimens of CF–3 cast SS, Heat No. P2 containing 15.6% ferrite (No. P2T–11), and Heat No. 69 containing 23.6% ferrite (Nos. 692–08B and 692–03B).
[b]Positive sawtooth wave form was used.
[c]Effluent dissolved-oxygen concentrations.
[d]Stress intensity K_{max} values at the end of the time period.

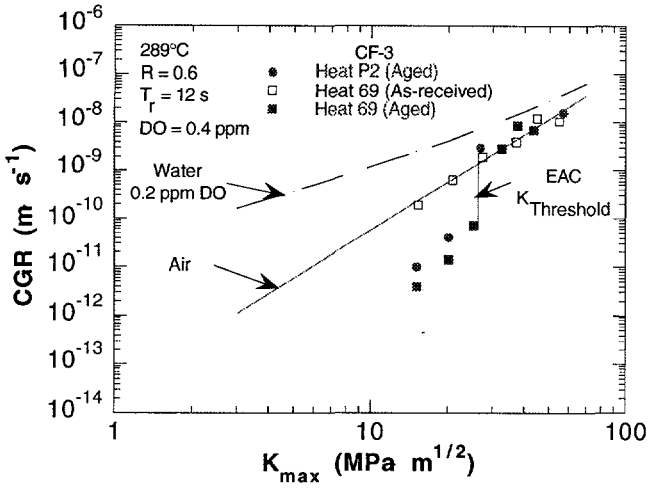

Figure 15.
Dependence of CGR of as-received and thermally aged CF-3 SS on K_{max} in HP oxygenated water at 289°C. Dashed and solid lines represent model predictions in water containing 0.2 ppm DO and in air, respectively, at R value of 0.6 and rise time of 12 s.

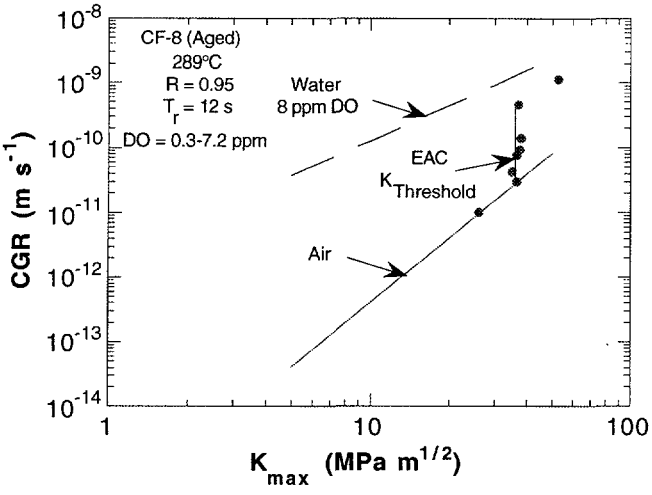

Figure 16.
Dependence of CGR of aged CF-8 SS on K_{max} in HP oxygenated water at 289°C. Dashed and solid lines represent model predictions in water containing 8 ppm DO and in air, respectively, at R value of 0.95 and rise time of 12 s.

decreases, CGRs in water and air increase and the difference in the rates becomes smaller at a given K_{max} value.

3.1.3 Dependence of Threshold Stress Intensity for EAC of Austenitic SSs on Load Ratio in 289°C Oxygenated Water

The dependence of the threshold stress intensity for EAC (K_{th}^{EAC}) and ΔK_{th}^{EAC}, where $\Delta K_{th}^{EAC} = K_{th}^{EAC}(1 - R)$, for specimens of Types 347, 316NG, and sensitized 304 SS and thermally aged CF-3 and CF-8 grades of cast SS on load ratio is shown in Figs. 17 and 18, respectively. These figures summarize data obtained in HP water containing 0.4–9.0 ppm DO at 289°C at load ratios between 0.2 and 0.95. At a given load ratio, the curves in Figs. 17 and 18 delineate the regimes where CGRs follow either the air line, i.e., to the left of the K_{th}^{EAC} and ΔK_{th}^{EAC} curves, or the water line at higher K_{max} and ΔK values. At K_{max} values <20 MPa·$m^{1/2}$, where EAC in not significant, CGRs in water lie below model predictions in water[44] by factors of ≈10 and 100 at load ratios of 0.6 and 0.95, respectively, as shown in Figs. 15 and 16. Thus, based on the present results, it may be more appropriate to utilize the air line when assessing crack growth of these

steels in water for K_{max} values below ≈20 MPa·m$^{1/2}$. The dependence of ΔK_{th}^{EAC} on load ratio in Fig. 18 is given by the equation

$$\Delta K_{th}^{EAC} = 25.0(1 - R). \quad (1)$$

Because of the break in the curve in Fig. 17, K_{th}^{EAC} may be somewhat lower than the value obtained from Eq. 1 at high load ratios, i.e., for R ≈1, K_{th}^{EAC} is ≈25 MPa·m$^{1/2}$, whereas the results in Fig. 17 suggest a lower value of ≈20 MPa·m$^{1/2}$. Several additional tests will be performed to determine the applicability of the relatively simple dependence of the EAC threshold on load ratio for all of the steels in oxygenated water. The CGR model for austenitic SSs in high-temperature water[44] will be revised to incorporate appropriate relations for the threshold stress intensity for EAC.

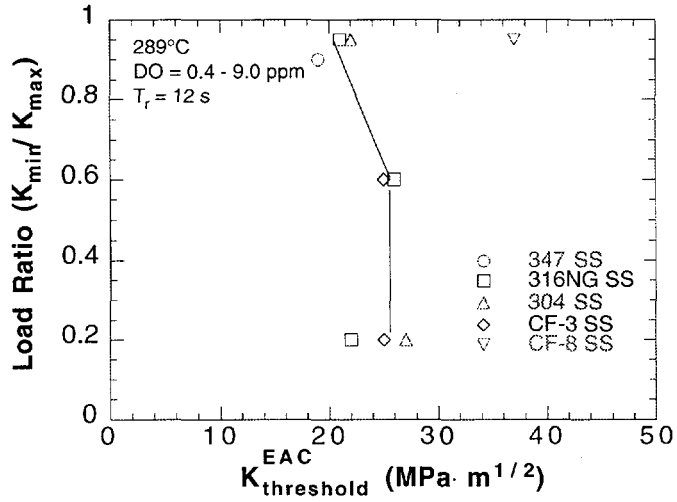

Figure 17. Dependence of K_{th} for EAC of wrought and cast austenitic SSs in HP oxygenated water at 289°C on load ratio

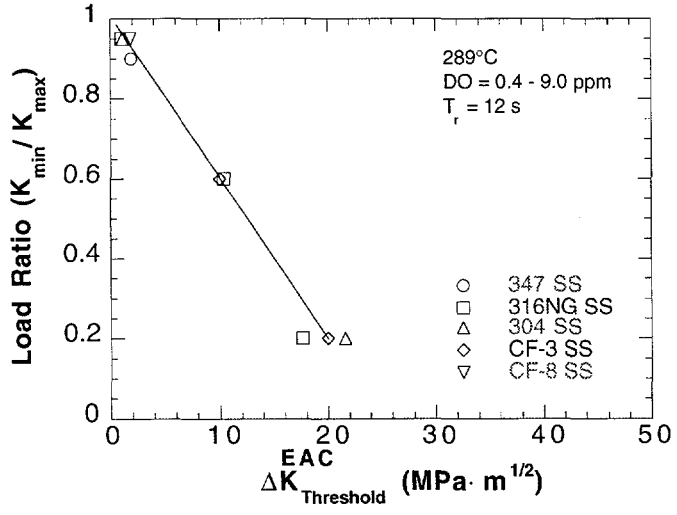

Figure 18. Dependence of ΔK_{th} for EAC of wrought and cast austenitic SSs in HP oxygenated water at 289°C on load ratio

3.1.4 Morphology of Crack Path and Surface of Stainless Steel CGR Specimens

The morphologies of corrosion-fatigue cracks in the wrought and cast austenitic SS specimens listed in Tables 4–6 have been determined. The 1T–CT specimens were sectioned vertically, and one-half of each specimen was split in the plane of the crack in

liquid nitrogen. The corrosion-product film was removed from the fracture surface by a chemical process to reveal the morphology of the underlying material. The intact portion of the specimen that encompassed the crack was polished and etched to corroborate the mode of crack propagation and also to determine if crack branching had occurred during the test. The total crack lengths at the end of the test were compared with values obtained by the dc potential-drop technique.

Figures 19–21 show the fracture surface, fracture morphology, and crack path in the crack-tip region of three Type 316NG SS specimens that were used in the corrosion fatigue experiments at a load ratio of 0.6 in HP water containing ≈6 ppm DO at 289°C (Table 4). The crack path and fracture morphology of these specimens and another Type 316NG SS specimen (Fig. 22) from experiments at a load ratio of 0.2 in HP water containing ≈9 ppm DO at 289°C (Table 5) reveal a transgranular mode of crack propagation. The wide crack opening in the crack-tip region of several of the specimens (e.g., Figs. 19, 21, and 22) was caused by the large stress intensity factors (43–74 $MPa \cdot m^{1/2}$) at the end of the experiments. The crack morphology shown in Fig. 23, for the lightly sensitized (EPR = 2 $C \cdot cm^2$) Type 304 SS specimen in the experiments at a load ratio of 0.2, was also transgranular.

TYPE 316NG SS	HEAT TREATMENT	LOAD CONDITIONS	ENVIRONMENT
Spec. No. CTD 198-3	1050°C for 0.5h plus	K_{max} = 5–74 $MPa \cdot m^{1/2}$	HP Water; 6 ppm DO
Heat No. 13198	650°C for 24 h	R = 0.6; Freq. = 0.077 Hz	289°C

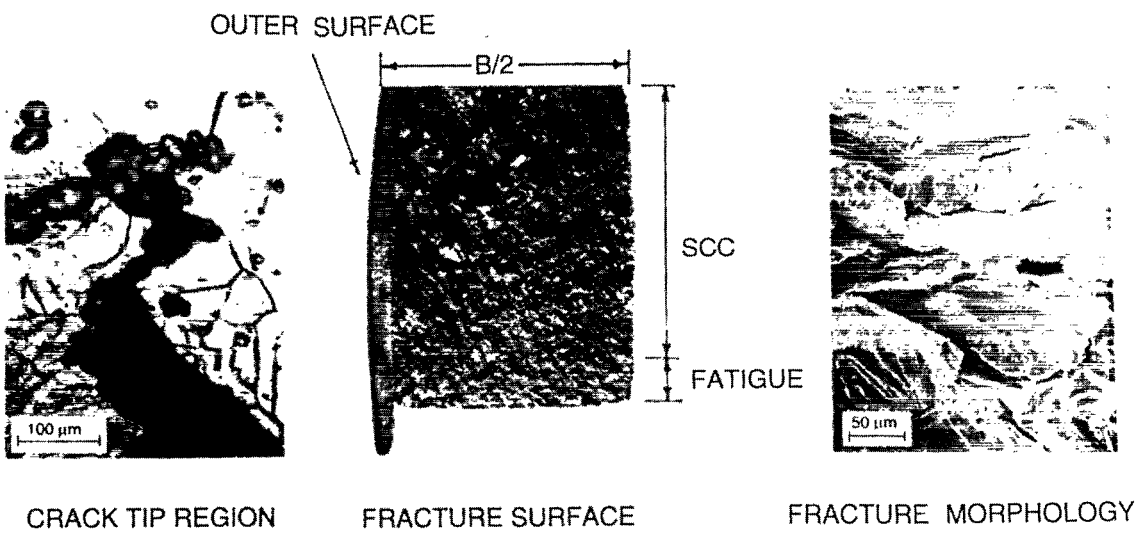

Figure 19. Crack path, fracture surface, and fracture morphology of 1T-CT specimen of Type 316NG SS (No. CTD-198-03) after crack growth experiment in HP water at 289°C

The crack morphologies of thermally aged and as-received cast CF-3 specimens that were tested in HP water containing either ≈9 ppm DO at a load ratio of 0.2 (Fig. 24, Table 5) or ≈0.4 ppm DO at a load ratio of 0.2 (Figs. 25–27, Table 6) are transgranular. The crack paths in these specimens traverse the austenite grains, in contrast to

TYPE 316NG SS	HEAT TREATMENT	LOAD CONDITIONS	ENVIRONMENT
Spec. No. CTD 4–1	1050°C for 0.5h plus	K_{max} = 5–38 MPa·m$^{1/2}$	HP Water; 6 ppm DO
Heat No. D432804	650°C for 24 h	R = 0.6; Freq. = 0.077 Hz	289°C

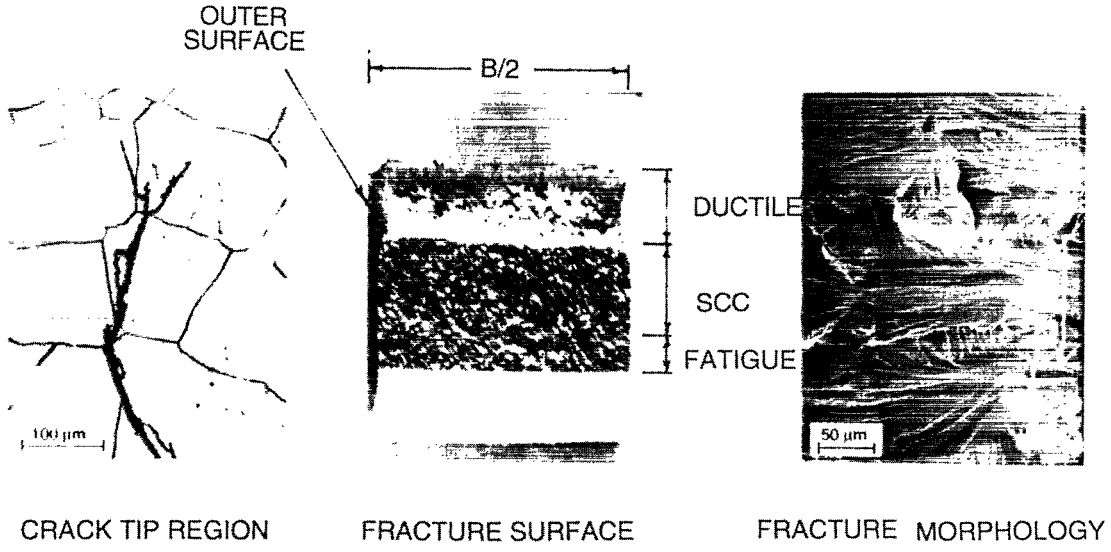

Figure 20. Crack path, fracture surface, and fracture morphology of 1T–CT specimen of Type 316NG SS (No. CTD–4–1) after crack growth experiment in HP water at 289°C

TYPE 316NG SS	HEAT TREATMENT	LOAD CONDITIONS	ENVIRONMENT
Spec. No. CTD 9–8	1050°C for 0.5h plus	K_{max} = 5–65 MPa·m$^{1/2}$	HP Water; 6 ppm DO
Heat No. P91576	650°C for 24 h	R = 0.6; Freq. = 0.077 Hz	289°C

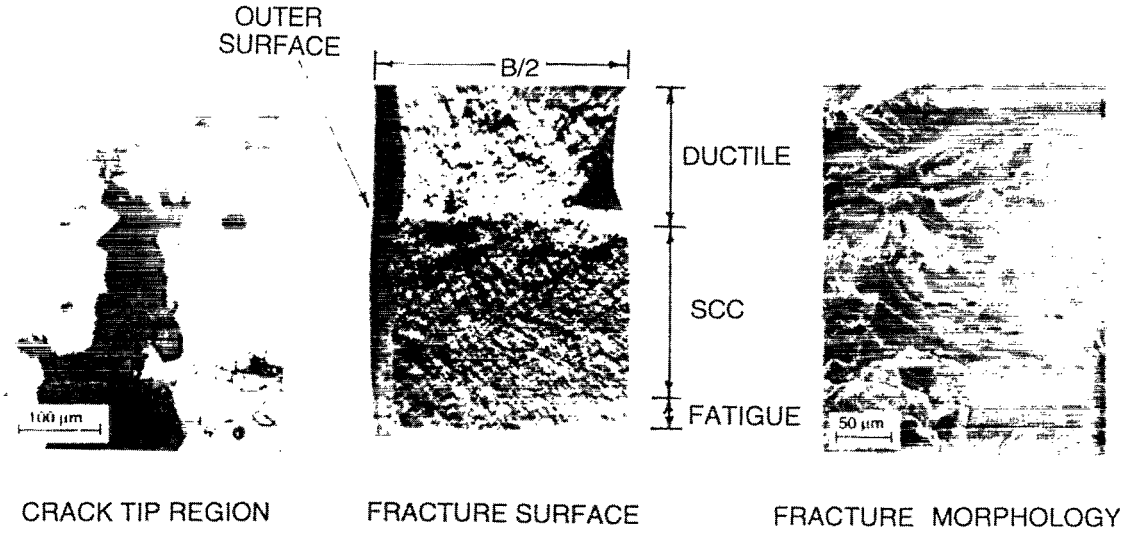

Figure 21. Crack path, fracture surface, and fracture morphology of 1T–CT specimen of Type 316NG SS (No. CTD–9–8) after crack growth experiment in HP water at 289°C

TYPE 316NG SS	HEAT TREATMENT	LOAD CONDITIONS	ENVIRONMENT
Spec. No. CTP 9–3	1050°C for 0.5h plus	K_{max} = 5–43 MPa·m$^{1/2}$	HP Water; 9 ppm DO
Heat No. P91576	650°C for 24 h	R = 0.2; Freq. = 0.077 Hz	289°C

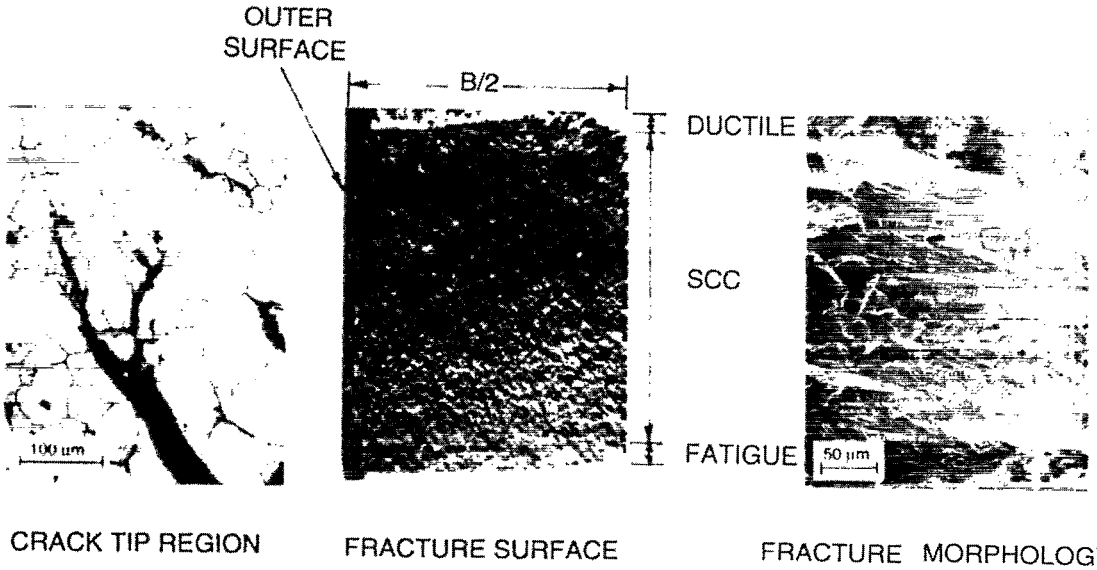

Figure 22. Crack path, fracture surface, and fracture morphology of 1T–CT specimen of Type 316NG SS (No. CTP 9–3) after crack growth experiment in HP water at 289°C

TYPE 304 SS	HEAT TREATMENT	LOAD CONDITIONS	ENVIRONMENT
Spec. No. 20	1050°C for 0.5h, 700°C	K_{max} = 5–50 MPa·m$^{1/2}$	HP Water; 9 ppm DO
Heat No. 30956	for 0.5 h, 500°C for 24 h	R = 0.2; Freq. = 0.077 Hz	289°C

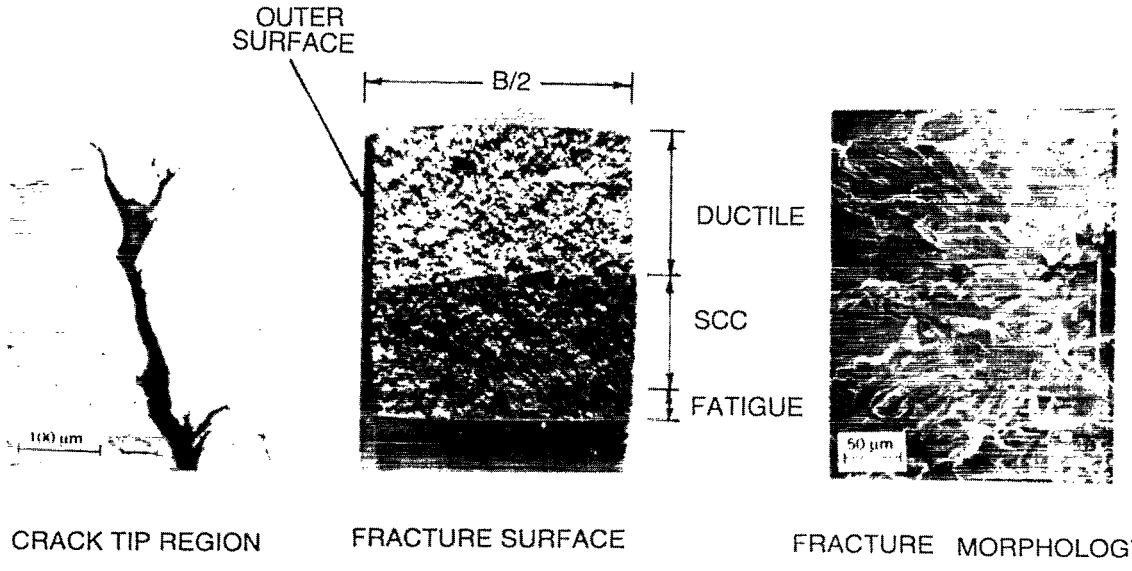

Figure 23. Crack path, fracture surface, and fracture morphology of sensitized 1T–CT specimen of Type 304 SS (No. 20) after crack growth experiment in HP water at 289°C

CF–3 SS	HEAT TREATMENT	LOAD CONDITIONS	ENVIRONMENT
Spec. No. P2T–12	350°C for 30,000 h	K_{max} = 5–54 MPa·m$^{1/2}$	HP Water; 9 ppm DO
Heat No. P2	in air	R = 0.2; Freq. = 0.077 Hz	289°C

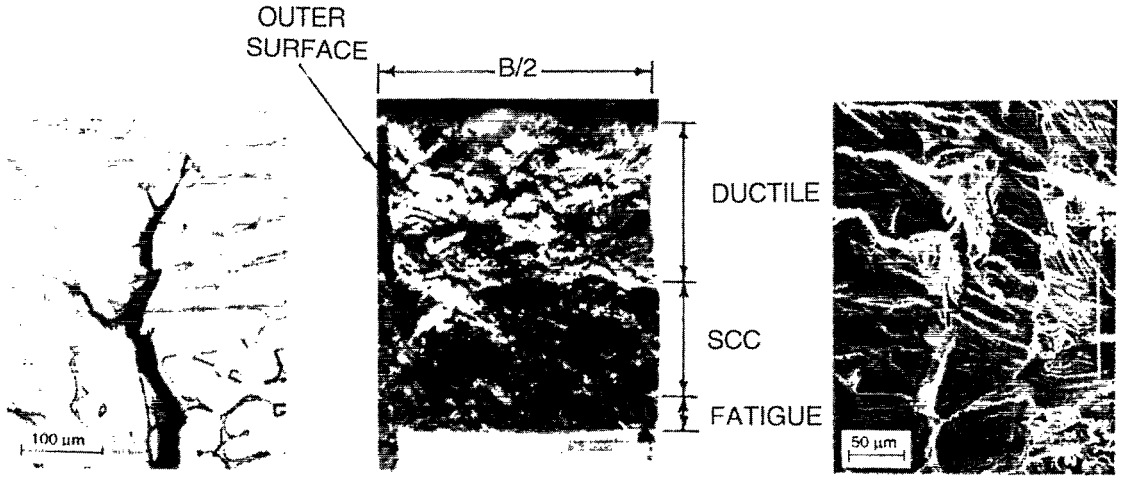

Figure 24. Crack path, fracture surface, and fracture morphology of thermally aged 1T–CT specimen of CF–3 SS (No. P2T–12) after crack growth experiment in HP water at 289°C

CF–3 SS	HEAT TREATMENT	LOAD CONDITIONS	ENVIRONMENT
Spec. No. P2T–11	350°C for 30,000 h	K_{max} = 15–56 MPa·m$^{1/2}$	HP Water; 0.4 ppm DO
Heat No. P2	in air	R = 0.6; Freq. = 0.077 Hz	289°C

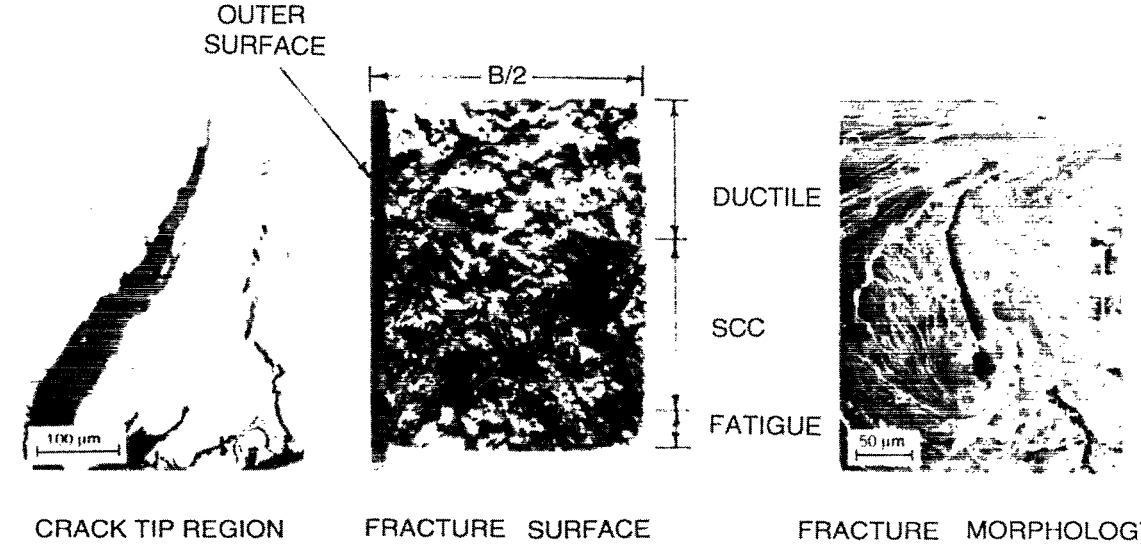

Figure 25. Crack path, fracture surface, and fracture morphology of thermally aged 1T–CT specimen of CF–3 SS (No. P2T–11) after crack growth experiment in HP water at 289°C

CF–3 SS	HEAT TREATMENT	LOAD CONDITIONS	ENVIRONMENT
Spec. No. 692–08B	As-received	K_{max} = 15–55 MPa·m$^{1/2}$	HP Water; 0.4 ppm DO
Heat No. 69		R = 0.6; Freq. = 0.077 Hz	289°C

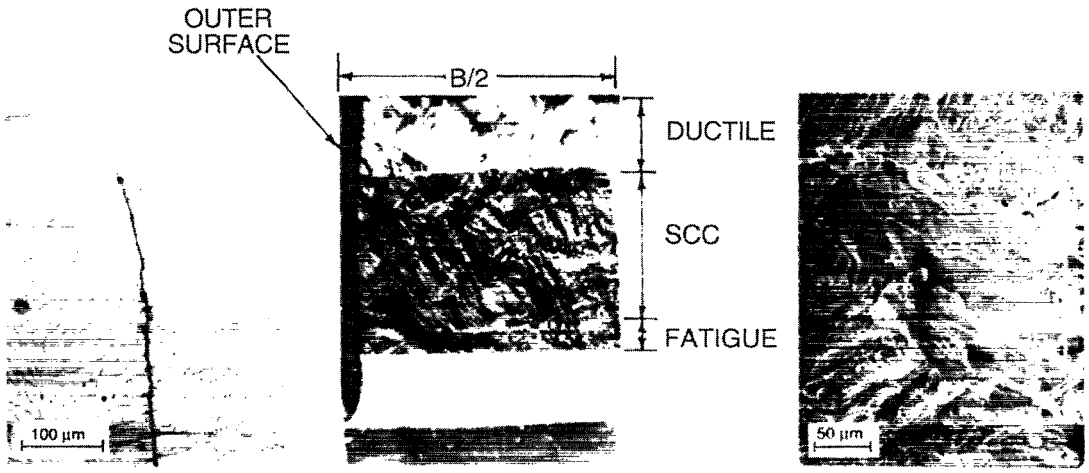

Figure 26. Crack path, fracture surface, and fracture morphology of as-received 1T–CT specimen of CF–3 SS (No. 692–08B) after crack growth experiment in HP water at 289°C

CF–3 SS	HEAT TREATMENT	LOAD CONDITIONS	ENVIRONMENT
Spec. No. 692–03B	350°C for 30,000 h	K_{max} = 15–44 MPa·m$^{1/2}$	HP Water; 0.4 ppm DO
Heat No. 69	in air	R = 0.6; Freq. = 0.077 Hz	289°C

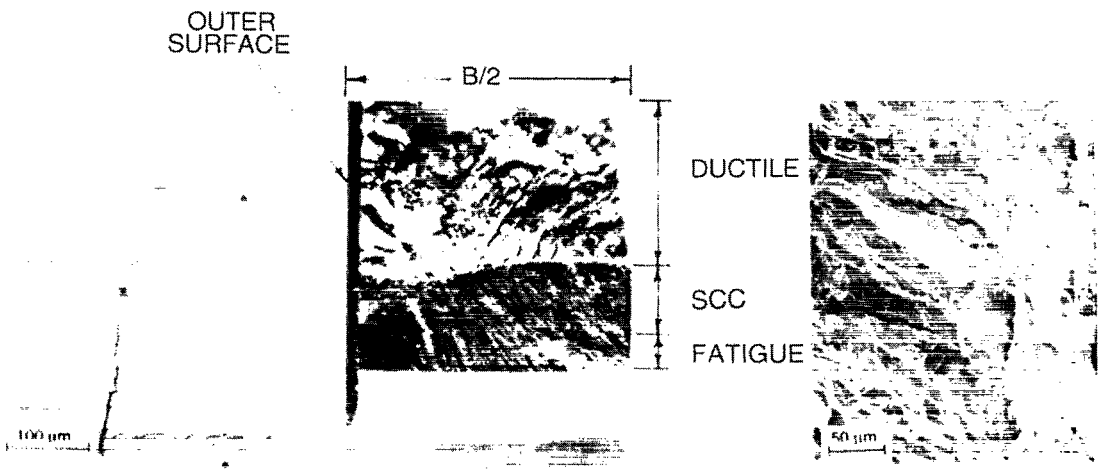

Figure 27. Crack path, fracture surface, and fracture morphology of thermally aged 1T–CT specimen of CF–3 SS (No. 692–03B) after crack growth experiment in HP water at 289°C

specimens from previous tests at a higher load ratio of 0.95,[45,47] where the cracks preferred the ferrite phase or ferrite/austenite phase boundaries. In the latter specimens, the path intersects austenite grains when their orientation would require the crack to deviate significantly from the crack plane. As the load ratio decreases from 0.95 to 0.6 and 0.2 at a $K_{max} > K_{th}^{EAC}$, the CGRs increase significantly (e.g., by factors of ≈10 and 100, respectively at a K_{max} of ≈40 MPa·m$^{1/2}$), which indicates that the mechanical contribution to crack propagation in oxygenated water at low load ratios increases at the expense of the environmental factor. This is consistent with the change in crack path and the more planar nature of the crack surfaces in specimens from experiments at load ratios ≤0.6.

4 Irradiation-Assisted SCC of Austenitic SSs

In recent years, failures of reactor-core internal components in both BWRs and PWRs have increased after accumulation of relatively high fluence (>5 x 10^{20} n·cm^{-2}, E >1 MeV). The general pattern of the observed failures indicates that, as nuclear plants age and neutron fluence increases, various apparently nonsensitized austenitic SSs become susceptible to intergranular failure. Some components (e.g., dry tubes, control-blade handle and sheath) are known to have cracked under minimal applied stress. Although most failed components can be replaced, some safety-significant structural components would be very difficult or impractical to replace. Therefore, the structural integrity of these components after accumulation of high fluence has been a subject of concern, and extensive research has been conducted to provide an understanding of this type of degradation, which is commonly known as IASCC.

In the mid-1960s, investigators began to implicate impurities, such as Si, P, and S in IASCC failure of components fabricated from solution-annealed nonsensitized austenitic SS. However, in direct contradiction of the earlier beliefs and initially encouraging test results obtained from HP Type 348 and 304 austenitic SSs, many investigators have reported slow-strain-rate-tensile (SSRT) and in-reactor test results which indicate that resistance of other HP heats (low in Si, C, P, and S) of Types 304 and 348 SS to IASCC failure is no better than that of CP materials. Therefore, the issue of superior performance of HP materials and the mechanisms of IASCC appear to be far from established. In general, heat-to-heat variation in susceptibility to IASCC has been very significant regardless of material grade, even among similar HP materials of virtually identical chemical composition. This seems to cast serious doubt not only on the role of grain-boundary segregation of impurities (i.e., Si, P, or S) but also on the premise that chromium depletion is the only important mechanism of IASCC. Although significant grain-boundary chromium depletion is believed by most investigators to play an important role (e.g., in thermally sensitized and irradiated components), it has been suspected that another primary process of IASCC of solution-annealed materials may be associated with other impurity elements (e.g., trace impurities) that are not specified in the ASTM specifications and that have been overlooked by most investigators. These elements are typically associated with iron and steel-making processes and with fabrication of the actual components, i.e., elements associated with flux compounds, cutting agents, recycled scrap, and strengthening materials. Some investigators suspect that hydrogen plays an important role through a yet-to-be-identified synergism in the process of IASCC.

In the following sections of this report, results of grain-boundary chemical analysis by Auger electron spectroscopy (AES) of Type 304 SS specimens from components irradiated in operating BWRs are examined further to determine the role of trace elements in promoting IGSCC in simulated BWR water. Other topics include: susceptibility of BWR irradiated Type 304 SS to hydrogen-induced intergranular fracture by mechanical loading in vacuo, status of fabrication of additional SSRT specimens from BWR neutron absorber rods, initial data that show the effects of electrochemical potential (ECP) and DO on IGSCC of specimens from BWR neutron absorber rods, and progress on assembly and calibration of a J-R test facility that will be used to determine fracture toughness of CT specimens irradiated in the Halden reactor.

4.1 Role of Trace Elements in SCC of Irradiated Austenitic SSs
(H. M. Chung, W. E. Ruther, and J. E. Sanecki)

In a previous publication,[48] we have reported initial results of AES analyses of trace elements (fluorine and vanadium) and a correlation of the results with susceptibility to IGSCC of Type 304 SS specimens (Table 1) irradiated in several BWRs to $\approx 2 \times 10^{21}$ n·cm^{-2} (E >1 MeV). The initial results indicated that susceptibility to IGSCC correlated well with grain-boundary concentrations of fluorine and vanadium. In this reporting period, more detailed analyses of fluorine have been conducted on ductile and intergranular fracture surfaces and on precipitates that were revealed by in-situ fracture of Types 304 and 348 SS specimens in the ultrahigh-vacuum environment of a scanning Auger microscope. The expanding-mandrel tube specimens from CP and HP heats of Type 348 SS, stressed by swelling of B_4C and Al_2O_3 pellets during irradiation in a fuel assembly in an operating BWR, were obtained from Siemens AG, Erlangen, Germany. Chemical composition, fluence, and susceptibility to cracking of the Type 348 SS tubes to IASCC have been reported in detail elsewhere by Garzarolli et al.[49-50] Fast-neutron fluence of IASCC-susceptible CP and IASCC-resistant HP heats of Type 348 SS was $\approx 1.5 \times 10^{21}$ and $\approx 3.5 \times 10^{21}$ n·cm^{-2} (E > 1 MeV), respectively. Chemical compositions of the two heats are given in Table 7.

Table 7. Chemical composition and fluence of HP and CP Type 304 and 348 SS BWR specimens analyzed by AES

Heat	Composition (wt.%)									Source	Service	Fluence
ID No.	Cr	Ni	Mn	C	N	B	Si	P	S	Code	Reactor	(10^{21} n·cm^{-2})
HP304-A	18.50	9.45	1.53	0.018	0.100	<0.001	<0.03	0.005	0.003	V-AT[a]	BWR-B	0.2-1.4
HP304-B	18.30	9.75	1.32	0.015	0.080	<0.001	0.05	0.005	0.005	V-AT[a]	BWR-B	0.2-1.4
HP304-CD	18.58	9.44	1.22	0.017	0.037	0.001	0.02	0.002	0.003	V-AT[a]	BWR-B	0.2-1.4
HP304-CD	18.58	9.44	1.22	0.017	0.037	0.001	0.02	0.002	0.003	QC-AT[a]	BWR-QC	2.0
CP304-A	16.80	8.77	1.65	0.08[b]	0.052	-	1.55	0.045[b]	0.030[b]	BL-AT[c]	BWR-Y	0.2-2.0
CP304-B	18.0-20.0	8-10.5	2.00[b]	0.08[b]	-	-	1.00[b]	0.045[b]	0.030[b]	LC-S[d]	BWR-LC	0.5-2.6
CP348a	17.4	11.5	1.56	0.074	0.042	-	0.34	0.007	0.009	SMT[e]	BWR-P	≈1.5
HP348b	17.7	11.1	1.65	0.041	0.008	-	0.19	0.002	0.007	SMT[e]	BWR-P	≈3.5

[a]HP neutron absorber tubes, OD = 4.78 mm, wall thickness = 0.63 mm, composition before irradiation.
[b]Represents maximum value in the specification; actual value not measured.
[c]CP absorber tubes, OD = 4.78 mm, wall thickness = 0.79 mm, composition after irradiation.
[d]CP control blade sheath, thickness = 1.22 mm; actual composition not measured.
[e]Swelling-mandrel tube irradiated in 7 x 7 fuel assembly in BWR KKP-1.

AES analysis of fluorine in SSs is inherently difficult because of the unique characteristics of Auger electrons of fluorine relative to those of iron. The primary Auger electron peak (derivative peak) for fluorine is at 650 eV and two minor peaks occur at 625 and 605 eV, respectively. The primary (650 eV) and secondary (605 eV) peaks of fluorine overlap with the primary (651 eV) and secondary (608 eV) peaks of iron, respectively. Because of this, it is easy to overlook the presence of fluorine at low concentration in steels by means of AES. However, at some locations on in-situ fracture surfaces of some BWR specimens, intensities of both 625- and 605-eV peaks were significantly high, and the presence of fluorine could be detected readily. This is shown in Fig. 28.

The 625-eV peak is unique to fluorine and absent in pure iron, either in N(E) or dN(E)/dE spectra. Therefore, a consistent linear correlation is expected between the intensities of the 605-eV (iron plus fluorine) and 625-eV (fluorine) peaks if fluorine is

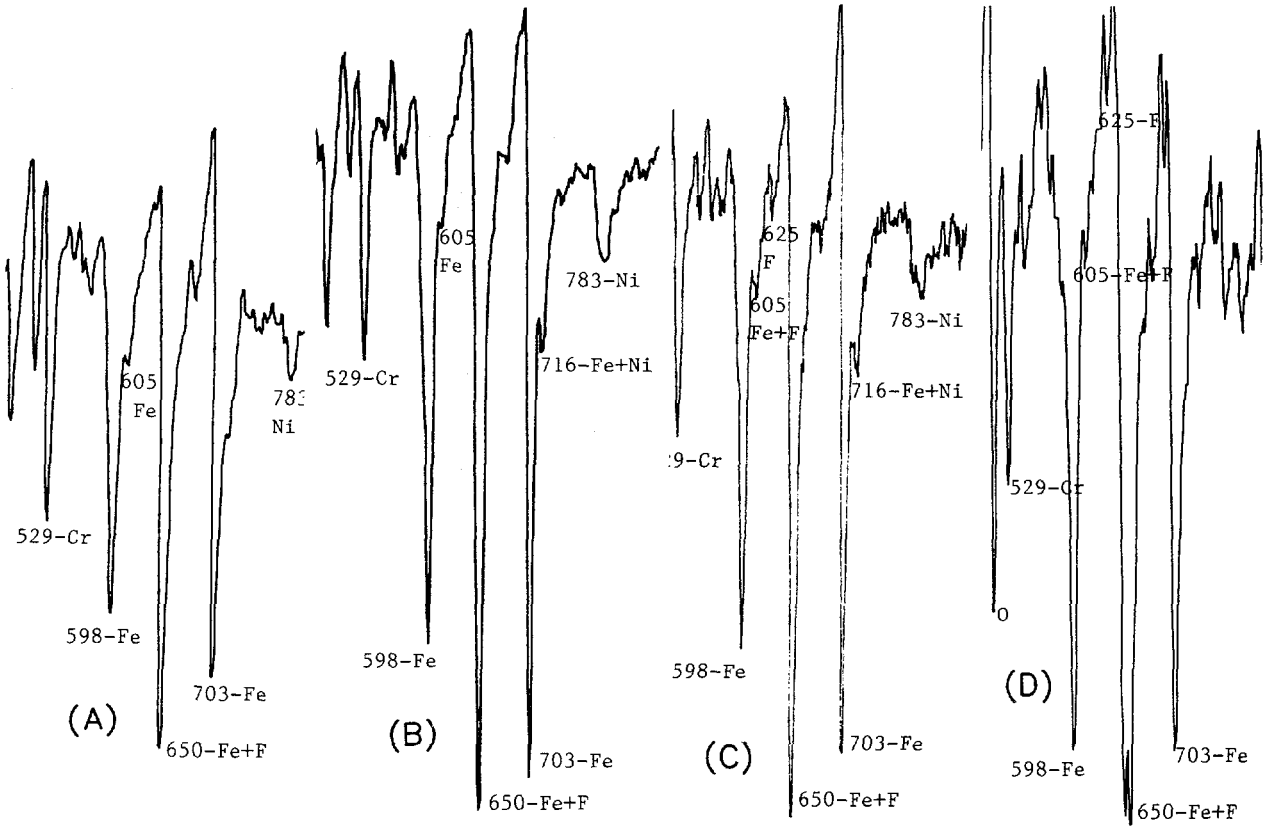

Figure 28. dN(E)/dE Auger electron spectra showing absence or presence of fluorine peaks (625- and 605-eV) from (A) nonirradiated Type 304 SS, ductile fracture surface; (B) BWR control-blade sheath, Type 304 SS, Heat CP304-B (Table 7), fluence ≈2 x 10^{21} n·cm^{-2}, intergranular fracture surface; (C) BWR neutron-absorber-rod tube, Type 304 SS, Heat CP304-A, fluence ≈2 x 10^{21} n·cm^{-2}, intergranular fracture surface; and (D) BWR swelling test tube, Type 348 SS, Heat 348a,[49-50] fluence ≈2.3 x 10^{21} n·cm^{-2}, ductile fracture surface. The primary peak of fluorine at 650 eV is hidden behind the 650-eV iron peak.

present in analyzed locations, as shown in Fig. 29. This figure shows that specimens obtained from BWR components contain trace amounts of fluorine at different levels. If fluorine was absent in the specimens, intensities of the 625–eV peak in Fig. 29 would be zero or negligible, as in the case of pure iron, regardless of the intensities of the 605–eV peak. An independent confirmation by means of a more sensitive chemical analysis is planned, even though trace amounts of halides in irradiated materials are known to be difficult to determine. At present, preparations are being made to analyze fluorine by glow–discharge mass spectrometry.

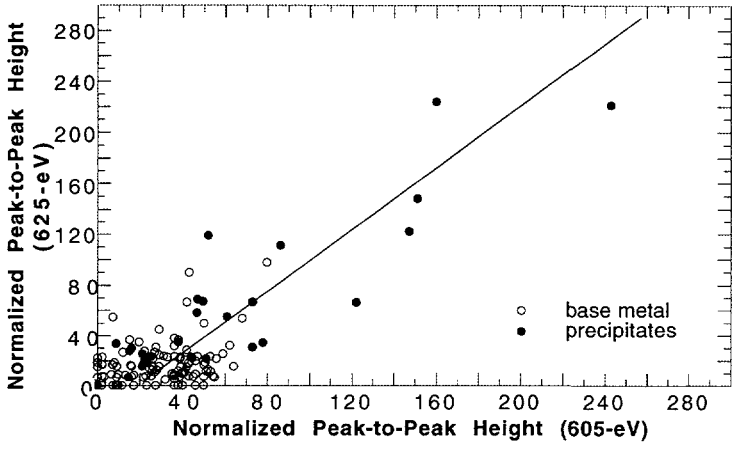

Figure 29.
Correlation of intensities from the 605–eV (Fe plus F) and 625–eV (F) AES peaks observed on ductile and intergranular fracture surfaces and precipitates in Type 304 and 348 SS specimens irradiated in BWRs

For comparison, Fig. 30 shows intensities of the 605– and 625–eV peaks for ductile fracture surfaces and various types of precipitates in the in–situ–produced fracture surfaces of Type 304 and 348 SS specimens. Essentially, four types of precipitates were identified by AES, i.e., MnS and CuS types in CP and HP Type 304 SS, and CuS, NbC, and M(S,F) types (M being iron and chromium) in CP and HP Type 348 SS specimens. In Fig. 30, fluorine trapping (i.e., a preferential partitioning of fluorine) in various types of precipitates is indicated by the somewhat higher intensities of the 605–eV (iron plus fluorine, left column) and 625–eV (fluorine, right column) peaks from precipitates compared with those of ductile surfaces. It seems that fluorine atoms are trapped strongly by sulfides but not by carbides. On the basis of these observations, the effect of fluorine on IGSCC is believed to be influenced not only by bulk concentration of fluorine in the steels but also by the type, number density, and volume fraction of precipitates that trap fluorine atoms.

The relative intensities of the 605–eV peak (fluorine plus iron), obtained from ductile (denoted by "D"), faceted, featureless (denoted by "U"), and intergranular (denoted by "I") fracture surfaces of CP and HP Types 304 SS BWR specimens irradiated to a fluence of $\approx 2 \times 10^{21}$ n·cm^{-2} (E >1 MeV), are shown in Fig. 31. In the figure, the right–hand–side graphs show results obtained from duplicate specimens. Similar results obtained from the 625–eV peak (fluorine) are shown in Fig. 32. The relative intensities from ductile and intergranular fracture surfaces of Figs. 31 and 32 indicate that fluorine segregation to grain boundaries, either by thermal or irradiation–induced processes, is negligible.

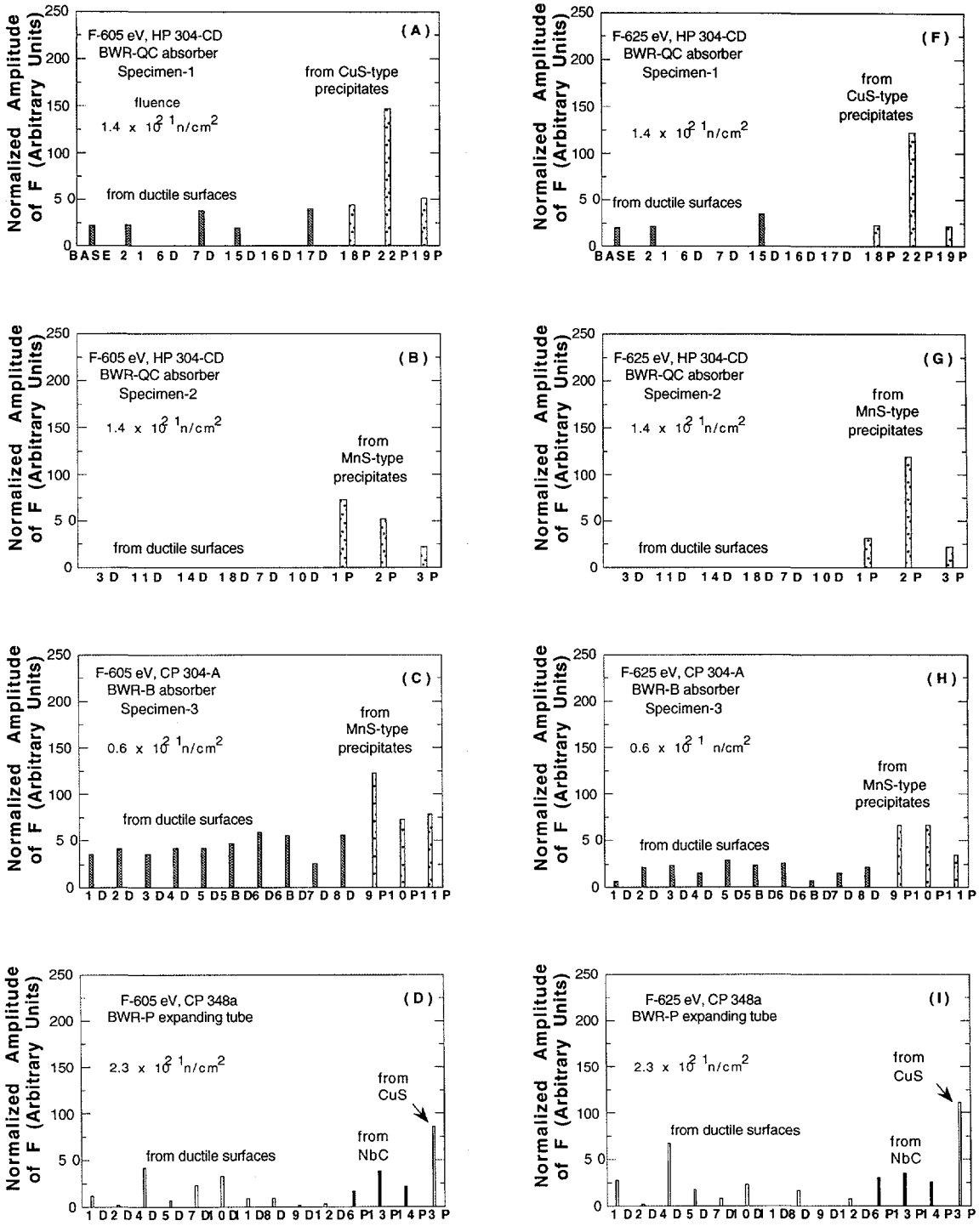

Figure. 30. Relative intensities of 605-eV peak (iron plus fluorine, left column) and 625-eV peak (fluorine, right column) from ductile surfaces (denoted by "D") and precipitates (denoted by "P") of CP and HP Type 304 and 348 SS BWR specimens

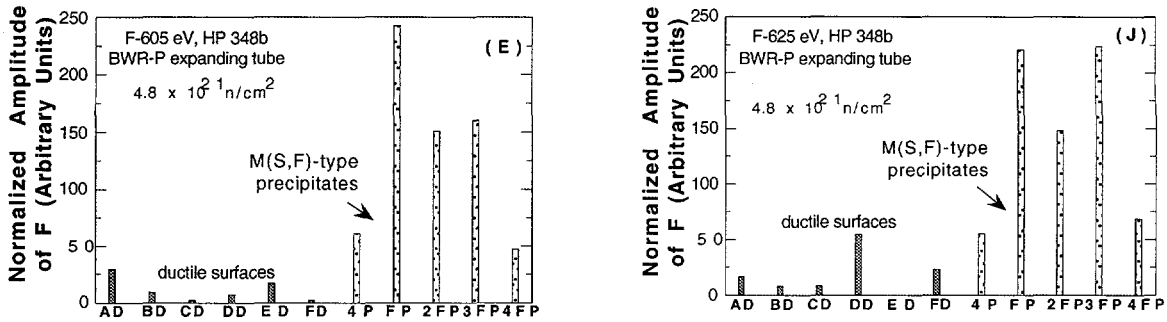

Figure 30. Continued

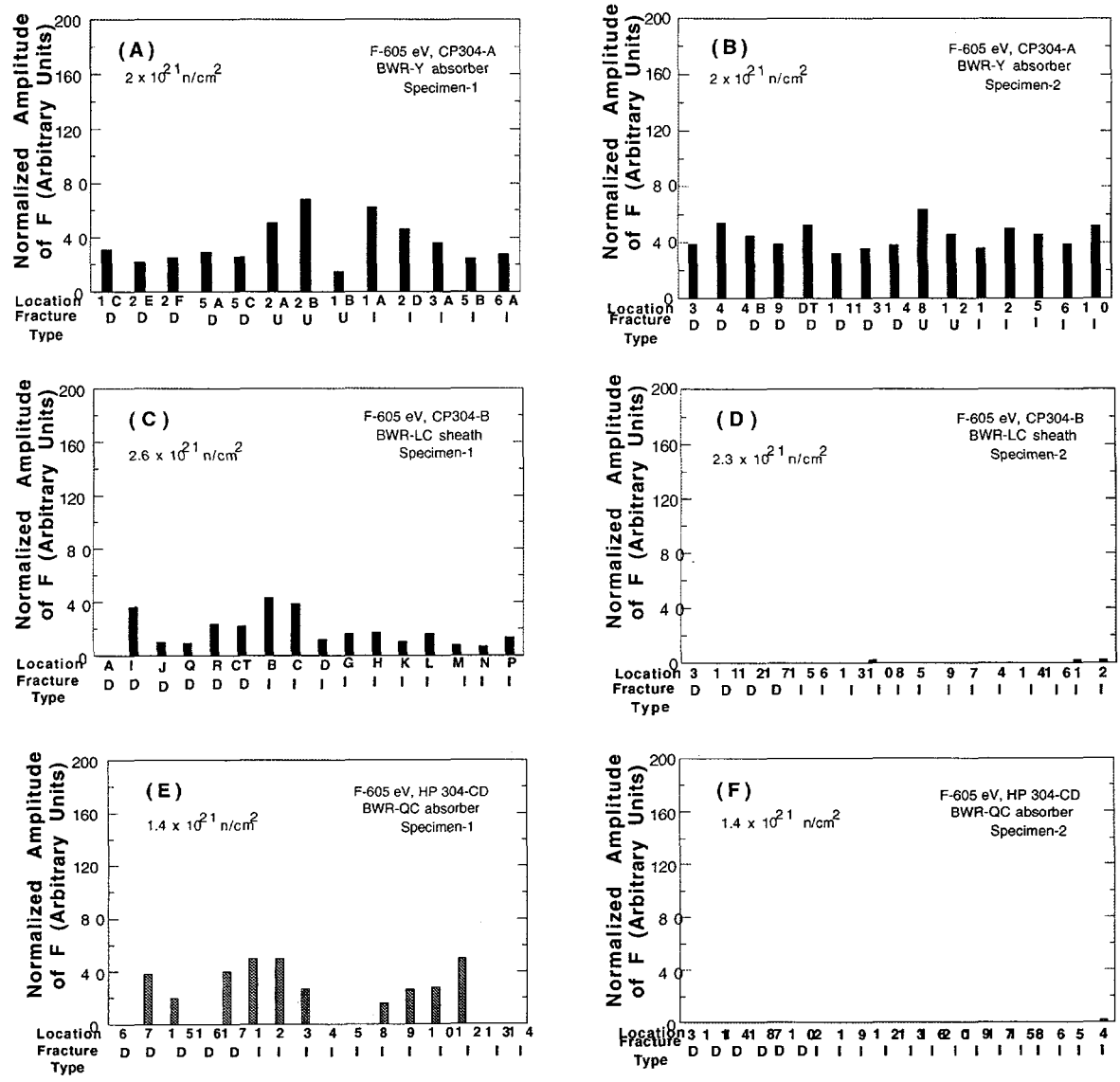

Figure 31. Relative intensities of 605-eV peak (fluorine plus iron) from ductile (denoted by "D"), intergranular ("I"), and faceted ("U") fracture surfaces of CP and HP Type 304 SS BWR specimens irradiated to ≈2 x 10^{21} n·cm^{-2}

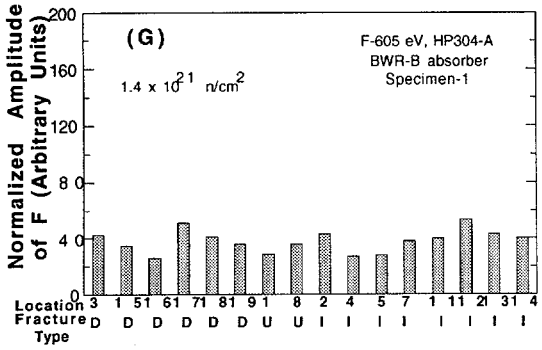

Figure 31. Continued

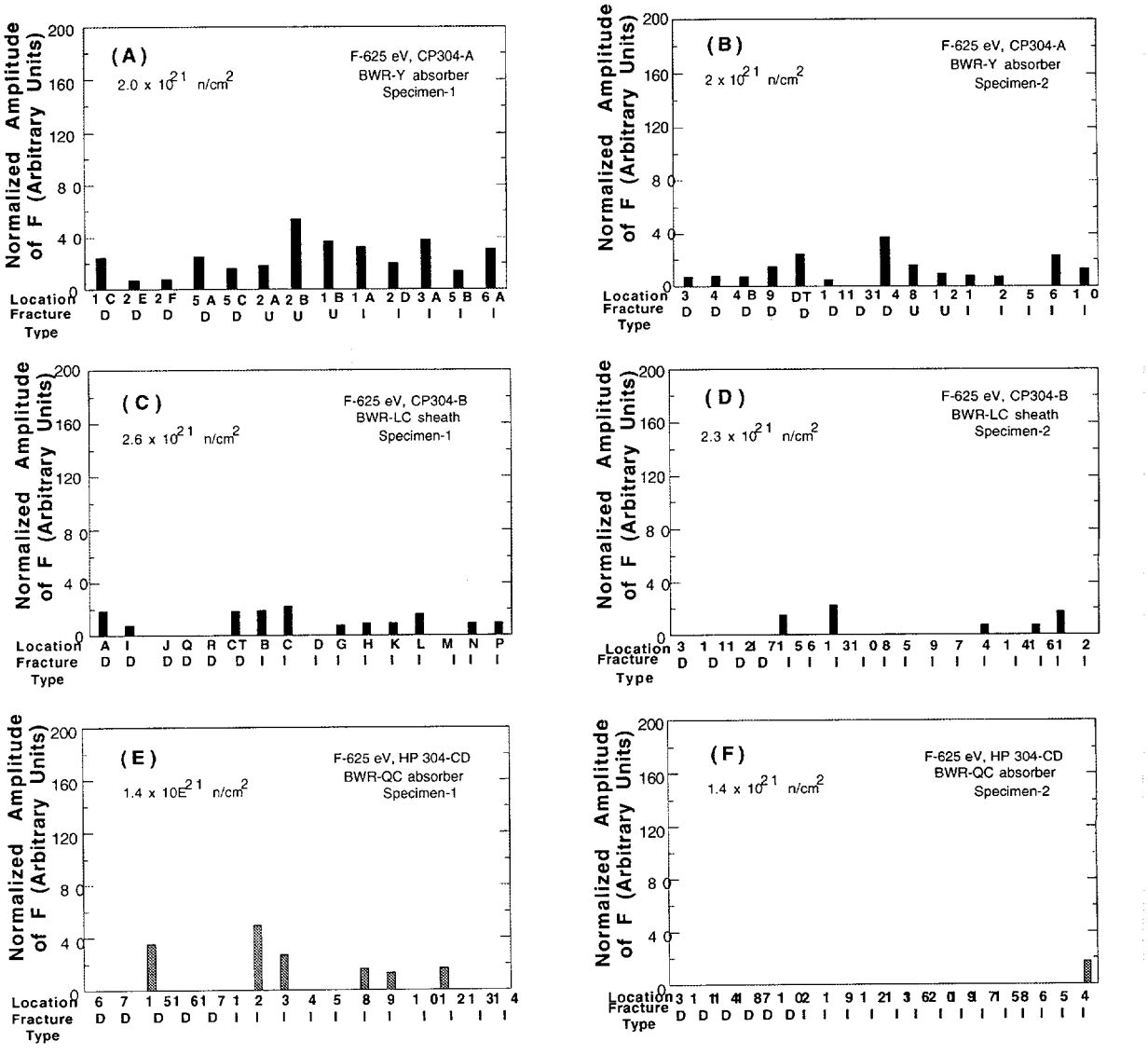

Figure 32. Relative intensities of fluorine signal (625 eV) from ductile (denoted by "D"), intergranular ("I"), and faceted ("U") fracture surfaces of CP and HP Type 304 SS BWR specimens irradiated to ≈2 x 10^{21} n·cm^{-2}

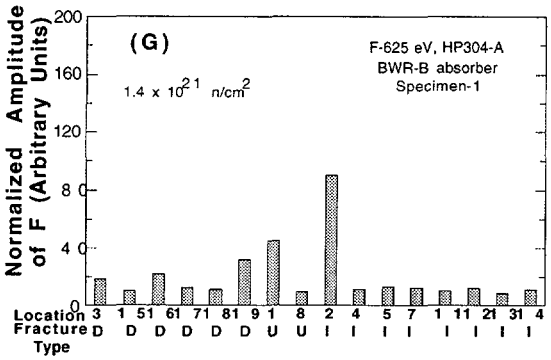

Figure 32. Continued

From the results shown in Figs. 31 and 32, intensities of the 605–eV peak (iron plus fluorine) and 625–eV peak (fluorine) were correlated with previously reported[51,52] susceptibilities of BWR specimens to IGSCC determined from SSRT tests. The correlations, shown in Figs. 33A and 33B, respectively, indicate a consistent pattern. That is, when fluorine is present in the steels above a certain level, susceptibility of the irradiated BWR specimens to IGSCC increases significantly.

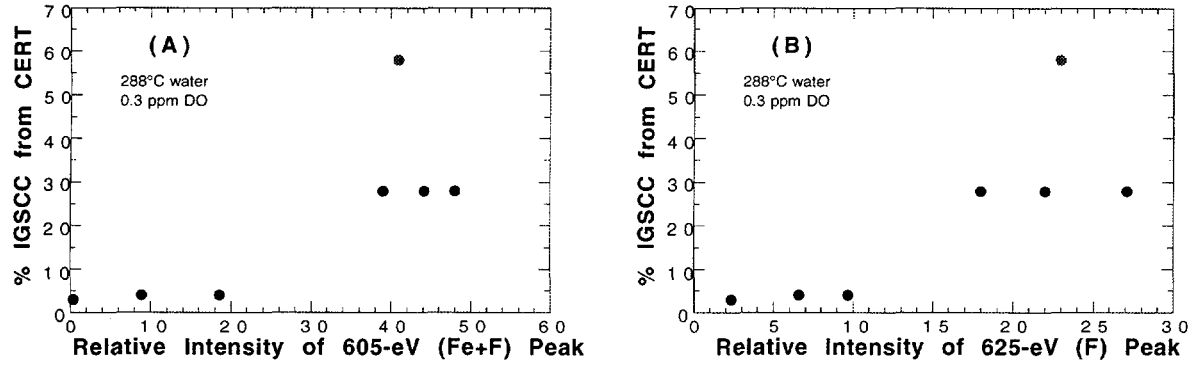

Figure 33. Relative intensities of the (A) 605–eV peak (iron plus fluorine) and (B) 625–eV peak (fluorine) vs. % IGSCC measured from SSRT tests of CP and HP Type 304 SS BWR specimens irradiated to ≈2 x 10^{21} n cm^{-2} (E >1 MeV)

On the basis of the present analysis of the effect of fluorine and the previously reported effect of grain–boundary chromium depletion,[51,52] it appears that for a similar level of hardening of the grain matrices by irradiation, a synergy of significant grain–boundary chromium depletion and a high fluorine level are conducive to a high susceptibility to IASCC. For example, the IASCC–resistant control blade sheath (Heat CP304–B, Table 7) was characterized by negligible grain–boundary chromium depletion and absence of fluorine in bulk (Figs. 31–33). On the other hand, the IASCC–susceptible neutron absorber tube (Heat HP304–A) was characterized by significant grain–boundary chromium depletion and relatively high level of fluorine.

A summary of the microchemical characteristics and susceptibility to IGSCC of the irradiated steels is given in Table 8. As reported previously,[51,52] the relative susceptibility to IGSCC could not be explained on the basis of grain–boundary segregation of Si or P. The relative susceptibility could be explained only with partial success on the

basis of grain-boundary depletion of chromium alone. The presence of fluorine and grain-boundary depletion of chromium accounts for the observed susceptibilities of all tested BWR specimens. For example, the IASCC-resistant control-blade sheath fabricated from a CP grade heat of Type 304 SS (CP304-B, Table 8) was virtually free of fluorine, and grain-boundary depletion of chromium in the heat was negligible. In contrast, the IASCC-susceptible neutron-absorber-rod tube fabricated from a HP grade heat of Type 304 SS (HP304-A) contained a relatively high level of fluorine, and grain-boundary depletion of chromium in the heat was significant.

Table 8. Summary of microchemical characteristics and susceptibility to IGSCC of CP and HP specimens of Type 304 SS from BWR components irradiated to a fluence of ≈2 x 10^{21} n·cm^{-2} (E >1 MeV)

Heat	Susceptibility	Grain-Boundary Cr Depletion[a]	Bulk Concentration of Fluorine	Bulk Concentration of Vanadium	Grain-Boundary Concentration of Silicon [a]	Grain-Boundary Concentration of Phosphorus[a]
CP304 -B	negligible [a]	negligible	negligible	negligible	high	high
HP304-CD	low [b]	significant	negligible	negligible	very low	very low
CP304-A	high [a]	medium	high	high	high	high
HP304-A	highest [a]	significant	high	high	very low	very low

[a]See Ref. 51
[b]See Refs. 53 and 54.

The present finding regarding the effect of fluorine contained in irradiated BWR specimens appears to be consistent with the effect of fluoride ions dissolved in water on the SCC of nonirradiated sensitized SS, which was reported by Ward et al.[55] In this study, fluoride ions as low as ≤1 ppm in water (25-82°C) were found to produce intergranular cracking in sensitized Types 304, 316, and 348 SS to varying degrees. However, solution-annealed steels and heat-affected zones near weldments were not susceptible under similar conditions. Besides sensitization, at least one or more of the following conditions were a prerequisite for intergranular attack: tensile stress (applied or residual); cold work; a crevice; and visible oxide film. Under some conditions (e.g., a thick oxide film), intergranular cracking occurred with negligible stress.

In irradiated steels, grain hardening (by neutron displacement damage) and grain-boundary depletion of chromium (by radiation-induced segregation) are always present to varying extents. It has been reported that irradiation hardening is significant for a fluence as low as ≈2 x 10^{20} n cm^{-2}, E >1 MeV (yield strength increases from ≈180-200 to 400-500 MPa).[52] It appears likely that a trace amount of fluorine in a crack-tip region in irradiated steels can enhance cracking along grain boundaries that are depleted of chromium.

Fluorine contamination can occur in SS components via the following routes.

- Fluorspar, ≈75% CaF_2, is a neutral flux used in production of crude iron and in steel-making processes. Steels with recycled fluorine-containing scrap would also inherit fluorine. Most stainless steels produced in the U.S. use recycled scrap.

- Flux in welding electrodes. Weld slag and welding fumes contaminate welds and the heat-affected zone with fluorine. Gas tungsten arc, plasma arc, and electron-beam welding do not use flux; thus they contribute no fluorine contamination. Most large

components (such as a BWR core shroud) are welded by submerged arc and shield-metal-arc processes because these processes are most practical and economical. However, these field processes use welding electrodes coated with fluorine-containing flux, and fluorine contamination from weld slag and welding fumes is possible.

- Pickling solutions that containing HF. Most small-tube components (e.g., BWR neutron-absorber-rod and dry tubes and PWR control-rod cladding) receive surface-finishing treatments after extrusion. After sand blasting, they are usually pickled in an HNO_3-HF solution to remove dirt, oil, and grease before shipping.

It is possible that the trace amounts of fluorine detected in BWR neutron-absorber-tube specimens analyzed in this study could have originated from an HNO_3-HF pickling solution. Such a contamination seems to be negligible in the control-blade sheath fabricated from sheet steel.

The mechanism whereby fluorine aggravates intergranular cracking is not known at this time. However, the process is believed to be associated with the presence of water and fluorine-containing compounds that react strongly with water. Ward et al. hypothesized that fluoride ions in water form soluble FeF_6 ions, which dissolve grain-boundary materials.[55] Another possibility, is that fluorine can combine with hydrogen to form HF molecules in the crack-tip region; HF will also react strongly with water. Vanadium pentafluoride (VF_5), a powerful oxidizing agent, readily forms at ≈300°C and is highly soluble in water.[56]

4.2 Effect of Water Chemistry on IASCC Susceptibility
(W. E. Ruther and H. M. Chung)

The effect of water chemistry on IASCC of BWR components has been assumed by many investigators to be similar to that for IGSCC of thermally sensitized austenitic SSs. However, data that show the influence of water chemistry on susceptibility of irradiated materials to IASCC are very limited, and it has not been well established that IASCC can be suppressed effectively by reducing the ECP of the material, and if so, what is the threshold level of the ECP. Data on effects of water chemistry on IASCC have been reported for only a few heats of Types 304 and 316 SS.[57-60]

To obtain a database on the effects of DO and water chemistry on susceptibility to IASCC, 31 SSRT specimens have been prepared from CP and HP Type 304 SS neutron-absorber-rod tubes irradiated in two BWRs. Boron carbide absorber was removed from the tube sections, and Swagelok fittings were attached to both ends of each tube section. The source of the heats (one CP and three HP) and fluence of the 31 specimens are summarized in Table 9.

Initial SSRT tests were conducted on several specimens listed in Table 9 to determine the effects of DO and ECP on time to failure, maximum stress, and total elongation. Neutron-absorber-rod tubes, fabricated from three similar heats of HP Type 304 SS and irradiated to a fluence of ≈1.4 x 10^{21} n·cm^{-2} (E > 1 MeV) in a BWR, were tested in HP water at 289°C at a DO level of ≈8 ppm. Details of the feedwater chemistry

Table 9. Source and fluence of 31 SSRT specimens of CP and HP Type 304 SS prepared from BWR neutron-absorber rods to determine effect of water chemistry on susceptibility to IASCC

SSRT Specimen Swagelok ID No.	Absorber Rod Tube Section Hot-Cell ID No.	Rod ID No. (BWR-Y) and Tube Section Axial Level (Inches from Bottom)	Rod ID No. (BWR-B) and Tube Section Axial Level (Inches from Top)	Source Stainless Steel Heat ID No.	Fast Neutron Fluence (10^{21} n·cm^{-2}) (E > 1 MeV)
20	389C2-1	4, 16-24		CP304-A	0.6
21	389C2-2	4, 16-24		CP304-A	0.6
22	389D2-1	5, 16-24		CP304-A	0.6
23	389D2-2	5, 16-24		CP304-A	0.6
24	389D3-1	5, 104-112		CP304-A	2.0
25	389D3-2	5, 104-112		CP304-A	2.0
26	389C3-1	4, 104-112		CP304-A	2.0
27	389C3-2	4, 104-112		CP304-A	2.0
28	389C1-1	4, 0-18		CP304-A	0.2
29	389C1-2	4, 0-18		CP304-A	0.2
30	389D1-1	5, 0-18		CP304-A	0.2
31	389D1-2	5, 0-18		CP304-A	0.2
32	A6A2-1		A6A, 0-8	HP304-A	1.4
33	A6A2-2		A6A, 0-8	HP304-A	1.4
34	473E-2		C4, 74-82	HP304-CD	0.7
35	389F2-1	18, 16-24		CP304-A	0.6
36	473E-1		C4, 74-82	HP304-CD	0.7
37	389F2-2	18, 16-24		CP304-A	0.6
38	473D-1		B5, 74-82	HP304-B	0.7
39	389F3-2	18, 104-112		CP304-A	2.0
40	389F3-1	18. 104-112		CP304-A	2.0
41	473D-2		B5, 74-82	HP304-B	0.7
42	473C-1		C6A, 0-8	HP304-CD	1.4
43	473C-2		C6A, 0-8	HP304-CD	1.4
44	473B-1		C5A, 0-8	HP304-CD	1.4
45	-		-	-	-
46	473B-2		C5A, 0-8	HP304-CD	1.4
47	473A-1		B7A, 0-8	HP304-B	1.4
48	473A-2		B7A, 0-8	HP304-B	1.4
49	B6A2-3		B6A, 0-8	HP304-B	1.4
50	B6A2-4		B6A, 0-8	HP304-B	1.4

and SSRT parameters are listed in Table 10. Chemical composition of the three heats (HP304-A, -B, and -CD, Table 7) is virtually identical, except for manganese and nitrogen levels. Results of the tests, shown in Fig. 34, seem to be very consistent.

In a previous test with a DO of ≈0.3 ppm, total elongation of an HP304-A specimen irradiated to a similar fluence was only ≈0.6%, somewhat lower than the present

Table 10. Results from SSRT[a] tests on specimens from three heats of HP Type 304 SS neutron absorber tubes in water containing ≈8 ppm DO at 289°C

SSRT No.	Swagelok Ident. No.	Source Heat Ident. No.	Source Rod and Section Ident. No.	Neutron Fluence E >1 MeV, 10^{21} n·cm^{-2}	α–γ Hot-Cell Ident. No.	Feedwater Chemistry: Oxygen Conc., ppm	Feedwater Chemistry: Average ECP mV SHE	Feedwater Chemistry: Cond. at 25°C, μS·cm^{-1}	Feedwater Chemistry: pH at 25°C	SSRT Parameters: Failure Time, h	SSRT Parameters: Max. Stress, MPa	SSRT Parameters: Total Elong., %
IR-41	32	HP304-A	A6A, 0–8	1.4	A6A2–1	8.3	156	0.120	6.35	34.7	414	2.06
IR-42	33	HP304-A	A6A, 0–8	1.4	A6A2–2	8.2	277	0.118	6.48	31.6	372	1.85
IR-43	47	HP304-B	B7A, 0–8	1.4	473A–1	8.9	165	0.118	6.49	31.9	383	1.91
IR-44	42	HP304–CD	C6A, 0–8	1.4	473C–1	8.2	122	0.084	6.80	30.8	360	1.83

[a]Strain rate of 1.65 x 10^{-7} s^{-1}.

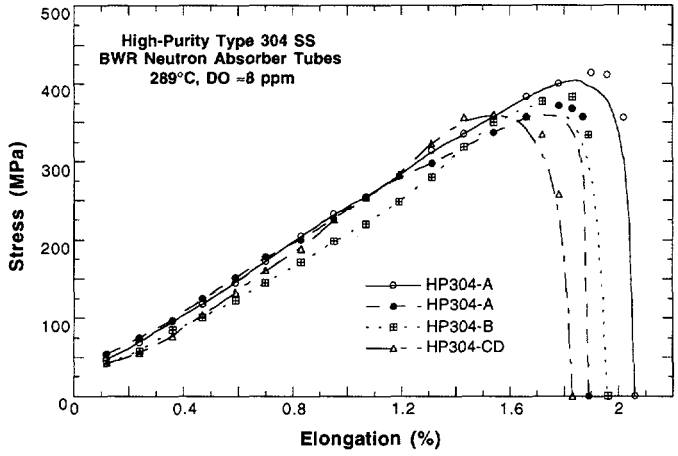

Figure 34. Stress vs. elongation from SSRT tests of three heats of HP Type 304 SS from BWR neutron absorber tubes irradiated to ≈1.4 x 10^{21} n·cm^{-2} (E > 1 MeV). Test was in simulated BWR water at 289°C, DO ≈8 ppm, and a strain rate of 1.65 x 10^{-7} s^{-1}.

elongation of ≈1.88%.[51] Although the elongation of both specimens was small, we would expect that a higher level of DO would produce a higher susceptibility to IASCC (i.e., lower total elongation). This trend is observed for IGSCC of nonirradiated sensitized commercial–purity materials. Based on a few tests, it appears that susceptibility of the irradiated HP heats is not significantly influenced by DO levels between ≈0.3 and 8 ppm, however, the database is insufficient and further tests must be conducted.

4.3 J–R Fracture Toughness Test of Irradiated Austenitic SS

(R. A. Erck, W. E. Ruther, and H. M. Chung)

Equipment is being built to perform in-cell J-R tests on miniature austenitic SS CT specimens by the dc potential–drop method. The miniature CT specimens, fabricated from several heats of Type 304 SS and irradiated to a fluence of ≈4.3 x 10^{20} n·cm^{-2}, have already been received from the Halden Reactor.

4.3.1 Facility

The system consists of a mobile tension test stand, furnace, and equipment rack. A schematic representation of the test stand is shown in Fig. 35. The hatched areas in the figure show the stressed members of the apparatus. Other members support the furnace assembly, which moves vertically on bearings to allow access to the specimen grips. An Instron 8500 servohydraulic control system has been acquired to operate the hydraulic cylinder.

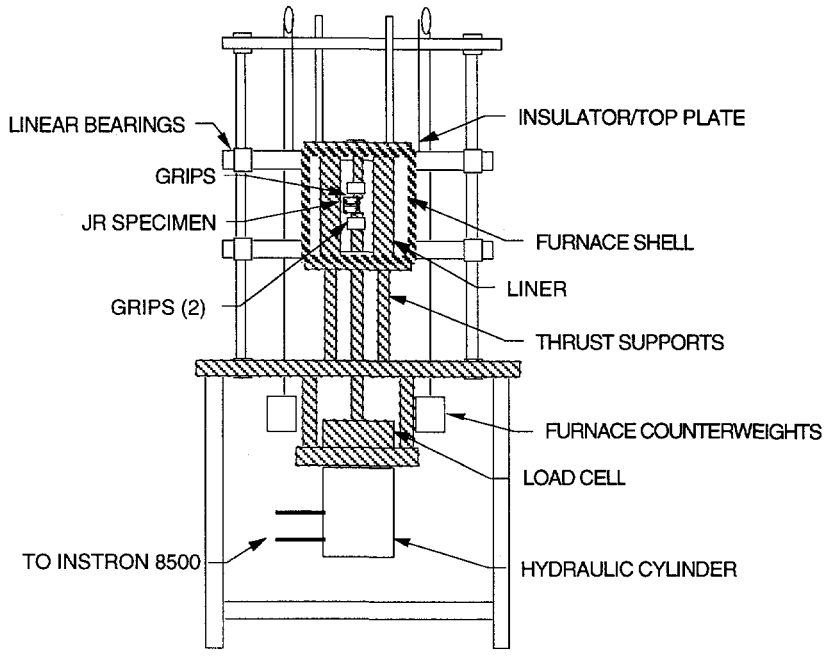

Figure 35. Schematic representation of J–R fracture-toughness facility for tests on miniature CT specimens of austenitic SS irradiated in the Halden HBWR

The dc potential–drop current is provided by a regulated power supply, and a Hewlett Packard 3457A microvoltmeter measures the generated potential. A PC computer, running a PASCAL program, is currently used for measurements of crack extension. The computer interfaces with a microvoltmeter via an IEEE 488 bus. The data-analysis program was written for standard–size tension specimens, but is readily adaptable to any size specimen by changing parameters.

Assembly and testing of the furnace has been completed, and stable operation to ±1°C at 288°C has been obtained. Temperature drift must be made as small as possible to minimize errors in the dc potential signals. The specimen is isolated from the ambient environment by a cylindrical thermal mass, with 50.8–mm bore, that is heated by the surrounding furnace.

We expect to acquire a more efficient and versatile program based on LabVIEW™ language, an icon-based programming language that can run on both IBM and Macintosh computers. The advanced program will be able to acquire data and communicate with the Instron 8500, thus allowing unattended operation.

The small specimen size makes remote attachment of the platinum current and potential wires (0.76 and 0.41 mm in diameter) difficult, especially with a remote manipulator. Originally, we thought that current and potential leads could be attached by small screws inserted into tapped holes in the CT specimen. A motorized jig for remotely attaching the screws was built, but this does not appear to be feasible. Instead, potential leads will be attached by means of tapered pins inserted into the angled holes that already exist in the specimen. Current leads will be attached by means of a spring

clip that is inserted from the back of the specimen. The placement of wires will conform to the ASTM draft recommendations for J-integral testing of CT specimens. The current will be introduced halfway along the width, and the potential will be measured at a distance one-sixth of the width from the midplane. Current and potential leads will be on the specimen centerline. This can be achieved if the existing tapped holes are used, and a clip is made for attaching the current leads. Based on finite-element methods, other investigators have concluded that current leads should be close to the crack tip and away from the potential leads.

4.3.2 Preliminary Test Results

Preliminary tests were conducted on nonirradiated Type 304 SS specimens at ambient temperature. These specimens were 50% cold-worked to simulate the embrittling effects of neutron irradiation. The specimens were similar in size and shape to the CT specimens irradiated in the Halden reactor, but the notch was square (not tapered), and no side groove was made. Current leads were spotwelded to the back of the specimen and potential was measured on the front. Specimens were strained in tension on an Instron machine. Number 32 drill rod was used to connect the CT specimen to the grips. During the test, a cobalt high-strength steel drill rod fractured under load, and subsequent tests were performed with a conventional drill rod. The crosshead speed was 8.3×10^{-4} mm·s^{-1}.

A program designed to acquire crack-extension data from nonirradiated 1T-CT specimens was used. After changing the program parameters to match the size of the miniature CT specimens, the crack length measured from the DC potential output was in good agreement with the actual crack length. The notch length was initially 5.9944 mm. Table 11 shows the applied force, measured resistance, and calculated crack length.

Table 11. Crack growth in cold-worked CT specimen of Type 304 SS

Test No.	Applied Force, kgf	Measured Resistance Ratio, Ω	Calculated Crack Length, mm
0	0	0.99659	5.9852
1	575	1.00055	6.0034
2	0	0.99286	5.9680
3	615	1.00781	6.0363
4	0	1.00200	6.0100
5	635	1.01377	6.0629
6	0	1.00322	6.0155
7	0	0.99624	5.9836
8	695	1.01486	6.0677
9	0	1.00009	6.0013
10	725	6.61591	fracture

The specimen was stressed with increasing force until fracture occurred (Fig. 36). During the test, small cracks emanated from the root of the notch but crack growth was negligible during the test. As the stress increased, a small increase in resistance (reversible) occurred. We believe that sensitivity to crack growth will be improved when current is introduced halfway along the width. Fracture of the specimen occurred instantaneously at 725 kgf.

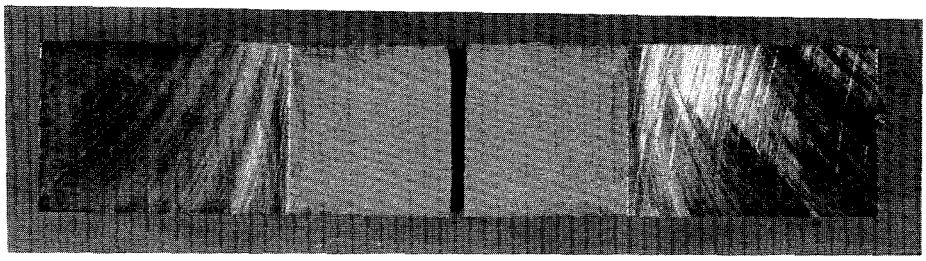

Figure 36. Appearance of crack opening in nonirradiated cold-worked Type 304 SS CT specimen (6.5 mm thick) fractured during calibration test of J-R apparatus

In the existing computer program, the calibration of resistance-vs.-crack length assumes that current is introduced at the back of the specimen, and that conventional specimen geometry is maintained. The CT specimens that were irradiated in the Halden reactor contain several tapped holes that were intended for wire attachment.[48] We expect that these holes will alter, albeit slightly, the current distribution in the specimen. The resistance-vs.-crack-length calibration must be established. Calibration will be performed by successively increasing the crack length by electrical-discharge machining, and resistance values will be obtained for each crack length. Alternatively, the specimen can be fatigued to grow the crack, and the precise crack length will be determined by a dye penetrant technique and postfracture examination.

5 Summary of Results

5.1 Fatigue of Ferritic Steels

- Fatigue tests have been conducted on A302-Gr B low-alloy steel to verify whether the current predictions of modest decreases of fatigue life in simulated PWR water are valid for high-sulfur heats that show environmentally enhanced fatigue CGRs in precracked specimens. The results indicate only a marginal effect of PWR water on fatigue life, i.e., life of A302-Gr B steel is lower by ≈23% in PWR water than in air at strain rates in tension of 0.4 and 0.004 %/s. Thus, even high-sulfur steels suffer only modest decreases of fatigue life in simulated PWR water.

- Fatigue tests were also conducted on A106-Gr B steel in high-DO water at 288°C and a strain range of ≈0.75% with 5- or 30-min hold periods at peak tensile strain. The results indicate that a tensile hold period decreases fatigue life in high-DO water but not in air. A 5-min hold period is sufficient to reduce fatigue life.

5.2 EAC of Wrought and Cast SSs in Simulated BWR Water

- Fracture-mechanics CGR tests were conducted on 1T-CT specimens of Types 316NG and 304 SS and as-received and thermally aged CF-3 cast SS to investigate threshold stress intensity factors K_{th}^{EAC} for EAC in HP oxygenated water at 289°C. The results were used to determine the dependence of K_{th}^{EAC} and ΔK_{th}^{EAC} on load ratio for wrought and cast austenitic SS specimens.

- Regimes were delineated where CGRs in water follow either the "air-line" in Section XI of the ASME Code at K_{max} and ΔK values below the threshold for EAC or ANL model predictions in water at higher stress intensity factors. At K_{max} values <20 MPa·$m^{1/2}$, where EAC in not significant, CGRs lie below ANL model predictions in water by factors of ≈10 and 100 at load ratios of 0.6 and 0.95, respectively.

- Based on the present results, it may be more appropriate to utilize the air line in the Code to assess crack growth of these steels in water at K_{max} values below ≈20 MPa·$m^{1/2}$. The ANL CGR model for austenitic SSs in high-temperature water will be revised to incorporate appropriate relations for the threshold stress intensity for EAC.

- Metallographic evaluation of the specimens after the experiments indicated that the mode of cracking in the wrought and cast specimens was transgranular at load ratios ≤0.6, and that the crack path in the cast SS specimens traversed the austenite grains in these tests, in contrast to previous tests at a load ratio of 0.95, in which the crack path preferred the ferrite/austenite phase boundaries in the cast materials. As the load ratio decreases from 0.95 to 0.6 and 0.2 at a $K_{max} > K_{th}^{EAC}$, the CGRs increase significantly, which indicates that the mechanical contribution to crack propagation increases at the expense of the environmental factor.

5.3 Irradiation-Assisted SCC of Type 304 SS

- A quantitative analysis of trace amounts of fluorine was conducted by AES on specimens from Type 304 and 348 SS BWR components. Fluorine contamination in the steels was analyzed from a secondary Auger electron peak that is unique to fluorine and does not overlap with Auger electron peaks of iron. Irradiated specimens from Type 304 SS heats that were more susceptible to IGSCC contained a higher level of fluorine than less susceptible heats. Fluorine content of sulfide precipitates was higher than that in either carbide precipitates or the grain matrices, indicating that fluorine is trapped by the former type of precipitates.

- The primary source of fluorine contamination in large BWR components, such as a core shroud, is believed to be weld fumes that originate from fluorine-containing weld flux (submerged arc and shielded metal arc). The primary source of fluorine contamination in tubular components, such as neutron-absorber-rod tubes, is the hydrofluoric acid-containing pickling solution that is used to clean these components.

- Susceptibilities of the HP and CP Type 304 SS materials from BWR components to IASCC in SSRT tests could be best explained on the basis of combined role of fluorine and grain-boundary depletion of chromium. The IASCC-resistant control blade sheath fabricated from a commercial-purity heat of Type 304 SS was virtually free of fluorine, and grain-boundary depletion of chromium in the heat was negligible. In contrast, an IASCC-susceptible neutron-absorber-rod tube fabricated from an HP heat of Type 304 SS contained a relatively high level of fluorine, and grain-boundary depletion of chromium in the heat was significant.

- More than 30 SSRT specimens were prepared from HP and CP Type 304 SS BWR neutron absorber tubes to test the effects of DO and water chemistry on susceptibility to IASCC. Several tests were conducted at a DO concentration of ≈8 ppm, and the results were compared with those obtained for a DO concentration of ≈0.3 ppm.

- A J–R test facility has been designed and assembled to measure fracture toughness of the miniature CT specimens irradiated in the Halden Reactor. Initial tests were conducted on nonirradiated cold–worked CT specimens of Type 304 SS. Good agreement was obtained between actual crack length and crack length determined from dc potential output obtained with an IBM–compatible PASCAL program.

References

1. K. Iida, *A Review of Fatigue Failures in LWR Plants in Japan*, Nucl. Eng. Des. **138**, 297–312 (1992).

2. *ASME Boiler and Pressure Vessel Code Section III – Rules for Construction of Nuclear Power Plant Components*, The American Society of Mechanical Engineers, 345 East 47th Street, New York, NY 10017.

3. *Criteria of Section III of the ASME Boiler and Pressure Vessel Code for Nuclear Vessels*, The American Society of Mechanical Engineers, United Engineering Center, New York, Library of Congress Catalog No. 56–3934 (1989).

4. *Tentative Structural Design Basis for Reactor Pressure Vessels and Directly Associated Components (Pressurized, Water Cooled Systems)*, PB 151987, U.S. Department of Commerce, Office of Technical Service, 1 Dec. 1958 Revision.

5. D. A. Hale, S. A. Wilson, E. Kiss, and A. J. Gianuzzi, *Low Cycle Fatigue Evaluation of Primary Piping Materials in a BWR Environment*, GEAP–20244, U.S. Nuclear Regulatory Commission (Sept. 1977).

6. D. A. Hale, S. A. Wilson, J. N. Kass, and E. Kiss, *Low Cycle Fatigue Behavior of Commercial Piping Materials in a BWR Environment*, J. Eng. Mater. Technol. **103**, 15–25 (1981).

7. S. Ranganath, J. N. Kass, and J. D. Heald, *Fatigue Behavior of Carbon Steel Components in High–Temperature Water Environments*, in Low–Cycle Fatigue and Life Prediction, ASTM STP 770, C. Amzallag, B. N. Leis, and P. Rabbe, eds., American Society for Testing and Materials, Philadelphia, PA, pp. 436–459 (1982).

8. S. Ranganath, J. N. Kass, and J. D. Heald, *Fatigue Behavior of Carbon Steel Components in High–Temperature Water Environments*, in BWR Environmental Cracking Margins for Carbon Steel Piping, EPRI NP–2406, Electric Power Research Institute, Palo Alto, CA, Appendix 3 (May 1982).

9. J. B. Terrell, *Fatigue Life Characterization of Smooth and Notched Piping Steel Specimens in 288°C Air Environments*, NUREG/CR–5013, EM–2232 Materials Engineering Associates, Inc., Lanham, MD (May 1988).

10. J. B. Terrell, *Fatigue Strength of Smooth and Notched Specimens of ASME SA 106–B Steel in PWR Environments*, NUREG/CR–5136, MEA–2289, Materials Engineering Associates, Inc., Lanham, MD (Sept. 1988).

11. J. B. Terrell, *Effect of Cyclic Frequency on the Fatigue Life of ASME SA–106–B Piping Steel in PWR Environments*, J. Mater. Eng. **10**,193–203 (1988).

12. P. D. Hicks, in *Environmentally Assisted Cracking in Light Water Reactors: Semiannual Report October 1990—March 1991*, NUREG/CR–4667 Vol. 12, ANL–91/24, pp. 3–18 (Aug. 1991).

13. P. D. Hicks and W. J. Shack, in *Environmentally Assisted Cracking in Light Water Reactors, Semiannual Report, April–September 1991*, NUREG/CR–4667 Vol. 13, ANL–92/6, pp. 3–8 (March 1992).

14. O. K. Chopra, W. F. Michaud, and W. J. Shack, in *Environmentally Assisted Cracking in Light Water Reactors, Semiannual Report, October 1992–March 1993*, NUREG/CR–4667 Vol. 16, ANL–93/27, pp. 3–19 (Sept. 1993).

15. O. K. Chopra, W. F. Michaud, W. J. Shack, and W. K. Soppet, in *Environmentally Assisted Cracking in Light Water Reactors, Semiannual Report, April–September 1993*, NUREG/CR–4667 Vol. 17, ANL–94/16, pp. 1–22 (June 1994).

16. M. Higuchi and K. Iida, *Fatigue Strength Correction Factors for Carbon and Low–Alloy Steels in Oxygen–Containing High–Temperature Water*, Nucl. Eng. Des. **129**, 293–306 (1991).

17. K. Iida, H. Kobayashi, and M. Higuchi, *Predictive Method of Low Cycle Fatigue Life of Carbon and Low Alloy Steels in High Temperature Water Environments*, NUREG/CP–0067, MEA–2090, Vol. 2, Materials Engineering Associates, Inc., Lanham, MD (April 1986).

18. N. Nagata, S. Sato, and Y. Katada, Low–Cycle Fatigue Behavior of Low–Alloy Steels in High–Temperature Pressurized Water, in *Transactions of the 10th International Conf. on Structural Mechanics in Reactor Technology*, F, A. H. Hadjian, ed., American Association for Structural Mechanics in Reactor Technology, Anaheim, CA (1989).

19. S. Majumdar, O. K. Chopra, and W. J. Shack, *Interim Fatigue Design Curves for Carbon, Low–Alloy, and Austenitic Stainless Steels in LWR Environments*, NUREG/CR–5999, ANL–93/3 (April 1993).

20. J. Keisler, O. K. Chopra, and W. J. Shack, *Statistical Analysis of Fatigue Strain–Life Data for Carbon and Low–Alloy Steels*, NUREG/CR–6237, ANL–94/21 (Aug. 1994).

21. L. A. James, *The Effect of Temperature and Cyclic Frequency Upon Fatigue Crack Growth Behavior of Several Steels in an Elevated Temperature Aqueous Environment*, J. Pressure Vessel Technol. **116**, 122–127 (1994).

22. O. K. Chopra and G. Ayrault, *Aging Degradation of Cast Stainless Steel: Status and Program*, Nucl. Eng. Des. **86**, 69-77 (1985).

23. H. M. Chung and O. K. Chopra, *Microstructures of Cast-Duplex Stainless Steels After Long-Term Aging*, in Proc. 2nd Int. Symp. on Environmental Degradation of Materials in Nuclear Power Systems - Water Reactors, Monterey, CA, The American Nuclear Society, La Grange Park, IL, pp. 287-292 (1986).

24. H. M. Chung and O. K. Chopra, *Long-Term Aging Embrittlement of Cast Austenitic Stainless Steels - Mechanisms and Kinetics*, in Properties of Stainless Steels in Elevated Temperature Service, M. Prager, ed., MPC-Vol. 26, PVP Vol. 132, American Society of Mechanical Engineers, New York, pp. 17-34 (1988).

25. H. M. Chung and O. K. Chopra, *Kinetics And Mechanisms of Thermal Aging Embrittlement of Duplex Stainless Steels*, in Proc. 3rd Int. Symp. on Environmental Degradation of Materials in Nuclear Power Systems - Water Reactors, Traverse City, MI, G. J. Theus and J. R. Weeks, eds., The Metallurgical Society, Warrendale, PA, pp. 359-370 (1988).

26. H. M. Chung, *Thermal Aging of Decommissioned Reactor Cast Stainless Steel Components and Methodology for Life Prediction*, Proc. 1989 ASME Pressure Vessel and Piping Conf., Honolulu, T. V. Narayana, et. al., eds., PVP Vol. 171, American Society of Mechanical Engineers, New York, pp. 111-115 (1989).

27. H. M. Chung, *Spinodal-like Decomposition of Austenite in Long-Term Aged Duplex Stainless Steel*, in Physical Metallurgy of Controlled Expansion Invar-Type Alloys, K. C. Russell and D. F. Smith, eds., The Minerals, Metals, and Materials Society, Warrendale, PA, pp. 129–141 (1990).

28. H. M. Chung and T. R. Leax, *Embrittlement of Laboratory- and Reactor-Aged CF-3, CF-8, and CF-8M Duplex Stainless Steels*, Mater. Sci. and Technol. **6**, 249–262 (1990).

29. H. M. Chung and O. K. Chopra, *Accelerated Aging Embrittlement of Cast Duplex Stainless Steel - Activation Energy for Extrapolation*, Proc. 4th Int. Symp. on Environmental Degradation of Materials in Nuclear Power Systems - Water Reactors, D. Cubicciotti, ed., National Association of Corrosion Engineers, Houston, pp. 3-47 to 3-65 (1990).

30. H. M. Chung, *Evaluation and Diagnosis of Aging of Cast Stainless Steel Components*, Proc. ASME Pressure Vessel and Piping Conf., PVP Vol. 208, American Society of Mechanical Engineers, New York, pp. 121-136 (1991).

31. H. M. Chung, *Aging and Life Prediction of Cast Duplex Stainless Steel Components*, Int. J. Pressure Vessel Piping **50**, 179–213 (1992).

32. W. F. Michaud, P. T. Toben, W. K. Soppet, and O. K. Chopra, Tensile–Property Characterization of Thermally Aged Cast Stainless Steels, NUREG/CR–6142, ANL–93/35 (Feb. 1994).

33. O. K. Chopra and H. M. Chung, *Aging of Cast Duplex Stainless Steels in LWR Systems*, Nucl. Eng. Des. **89**, 305-318 (1985).

34. O. K. Chopra and H. M. Chung, *Effects of Low Temperature Aging on the Mechanical Properties of Cast Stainless Steels*, in Properties of Stainless Steels in Elevated Temperature Service, M. Prager, ed., MPC-Vol. 26, PVP Vol. 132, American Society of Mechanical Engineers, New York, pp. 79-105 (1988).

35. O. K. Chopra and H. M. Chung, *Aging Degradation of Cast Stainless Steels: Effects on Mechanical Properties*, in Proc. 3rd Int. Symp. on Environmental Degradation of Materials in Nuclear Power Systems - Water Reactors, Traverse City, MI, G. J. Theus and J. R. Weeks, eds., The Metallurgical Society, Warrendale, PA, pp. 737-748 (1988).

36. O. K. Chopra and H. M. Chung, *Embrittlement of Cast Stainless Steels in LWR Systems*, Proc. 15th MPA-Seminar on Safety and Reliability of Plant Technology, Vol. 1, pp. 13.1-13.23 (1989).

37. O. K. Chopra, *Thermal Aging of Cast Stainless Steels: Mechanisms and Predictions*, in Fatigue, Degradation, and Fractures, W. H. Bamford, C. Becht IV, S. Bhandari, J. D. Gilman, L. A. James, and M. Prager, eds., PVP Vol. 195, The American Society of Mechanical Engineers, New York, pp. 193-214 (1990).

38. O. K. Chopra, *Thermal Aging of Cast Stainless Steels in LWR Systems: Estimation of Mechanical-Properties*, in Nuclear Plant Systems/Components Aging Management and Life Extension, PVP Vol. 228, American Society of Mechanical Engineers, New York, pp. 79–92 (1992).

39. O. K. Chopra, *Prediction of Aging Degradation of Cast Stainless Steel Components in LWR Systems*, in Proc. Aging Research Information Conf., NUREG/CP–0122 Vol. 2, pp. 324–340 (1992).

40. O. K. Chopra and W. J. Shack, *Evaluation of Aging Degradation of Structural Components*, in Proc. Aging Research Information Conf., NUREG/CP–0122 Vol. 2, pp. 369–386 (1992).

41. O. K. Chopra, *Long-Term Embrittlement of Cast Duplex Stainless Steels in LWR Systems: Semiannual Report, October 1990 – March 1991*, NUREG/CR–4744 Vol. 6, No 1, ANL–91/22 (Aug. 1992).

42. O. K. Chopra, *Long-Term Embrittlement of Cast Duplex Stainless Steels in LWR Systems: Semiannual Report, April – September 1991*, NUREG/CR–4744 Vol. 6, No 2, ANL–92/32 (Nov. 1992).

43. O. K. Chopra, *Long-Term Embrittlement of Cast Duplex Stainless Steels in LWR Systems: Semiannual Report, October 1991 – March 1992*, NUREG/CR–4744 Vol. 7, No 1, ANL–92/42 (May 1993).

44. W. J. Shack and T. F. Kassner, *Review of Environmental Effects on Fatigue Crack Growth of Austenitic Stainless Steels*, NUREG/CR–6176, ANL–94/1, (May 1994).

45. W. E. Ruther, O. K. Chopra, and T. F. Kassner, in *Environmentally Assisted Cracking in Light Water Reactors: Semiannual Report, April – September 1992*, NUREG/CR–4667 Vol. 15, ANL–93/2, pp. 21–28 (June 1993).

46. W. E. Ruther, O. K. Chopra, and T. F. Kassner, in *Environmentally Assisted Cracking in Light Water Reactors: Semiannual Report, October 1992 – March 1993*, NUREG/CR–4667 Vol. 16, ANL–93/27, pp. 19–27 (Sept. 1993).

47. W. E. Ruther and T. F. Kassner, in *Environmentally Assisted Cracking in Light Water Reactors: Semiannual Report, October 1992 – March 1993*, NUREG/CR–4667 Vol. 17, ANL–94/16, pp. 22–34 (June 1994).

48. H. M. Chung, W. E. Ruther, and J. E. Sanecki, in *Environmentally Assisted Cracking in Light Water Reactors: Semiannual Report April 1993-September 1993*, NUREG/CR-4667, Vol. 17, ANL-94/16, pp. 35-41 (June 1994).

49. F. Garzarolli, P. Dewes, R. Hahn, and J. L. Nelson, "*Deformability of High-Purity Stainless Steels and Ni-Base Alloys in the Core of a PWR*," Proc. 6th Int. Symp. Environmental Degradation of Materials in Nuclear Power Systems - Water Reactors, R. E. Gold and E. P. Simonen, Eds., The Minerals, Metals, and Materials Society, Warrendale, PA, pp. 607-613 (1993).

50. F. Garzarolli, D. Alter, P. Dewes, and J. L. Nelson, *Deformability of Austenitic Stainless Steels and Ni-Base Alloys in the Core of a Boiling and Pressurized Water Reactor*, Proc. 3rd Int. Symp. Environmental Degradation of Materials in Nuclear Power Systems - Water Reactors, G. J. Theus and J. R. Weeks, eds., The Metallurgical Society, Warrendale, PA, pp. 657-664 (1988).

51. H. M. Chung, W. E. Ruther, J. E. Sanecki, A. G. Hins, and T. F. Kassner, *Stress Corrosion Cracking Susceptibility of Irradiated Type 304 Stainless Steels*, Effects of Radiation on Materials: 16th Int. Symp., ASTM STP 1175, A. S. Kumar, D. S. Gelles, R. K. Nanstad, and T. A. Little, eds., American Society for Testing and Materials, Philadelphia, pp. 851-869 (1993).

52. H. M. Chung, W. E. Ruther, J. E. Sanecki, A. G. Hins, and T. F. Kassner, *Irradiation-Assisted Stress Corrosion Cracking of Materials from Commercial BWRs: Role of Grain-Boundary Microchemistry*, Proc. of 21st Water Reactor Safety Information Mtg., NUREG/CP-0133, Vol. 3, April 1994, pp. 135-152.

53. A. J. Jacobs, *The Relationship of Grain Boundary Composition in Irradiated Type 304SS to Neutron Fluence and IASCC*, Effects of Radiation on Materials: 16th International Symp., ASTM STP 1175, A. S. Kumar, D. S. Gelles, R. K. Nanstad, and T. A. Little, Eds., American Society for Testing and Materials, Philadelphia, 1993, pp. 902-918.

54. H. M. Chung, W. E. Ruther, J. E. Sanecki, and T. F. Kassner, *Grain-Boundary Microchemistry and Intergranular Cracking Of Irradiated Austenitic Stainless Steel*, Proc. 6th Int. Symp. Environmental Degradation of Materials in Nuclear Power Systems - Water Reactors, R. E. Gold and E. P. Simonen, eds., The Minerals, Metals, and Materials Society, Warrendale, PA, pp. 511-519.

55. C. T. Ward, D. L. Mathis, and R. W. Staehle, *Intergranular Attack of Sensitized Austenitic Stainless Steel by Water Containing Fluoride Ions*, Corrosion, 25 (1969), pp. 394-396.

56. *Extractive Metallurgy of Vanadium*, C. K. Gupta and N. Krishnamurthy, Elsevier Science, Amsterdam, 1992, pp. 395-397.

57. A. J. Jacobs, G. P. Wozaldo, K. Nakata, T. Yoshida, and I. Masaoka, *Radiation Effects on the Stress Corrosion and Other Selected Properties of Type-304 and Type-316 Stainless Steels*, Proc. 3rd Int. Symp. Environmental Degradation of Materials in Nuclear Power Systems – Water Reactors, G. J. Theus and J. R. Weeks, eds., The Metallurgical Society, Warrendale, PA, pp. 673–681 (1988).

58. M. E. Indig, J. L. Nelson, and G. P. Wozaldo, *Investigation of the Protection Potential Against IASCC*, Proc. 5th Int. Symp. Environmental Degradation of Materials in Nuclear Power Systems – Water Reactors, D. Cubicciotti, E. P. Simonen, and R. Gold, eds., American Nuclear Society, La Grange Park, IL, pp. 657–664 (1992).

59. M. Kodama, S. Nishimura, J. Morisawa, S. Shima, S. Suzuki, and M. Yamamoto, *Effects of Fluence and Dissolved Oxygen on IASCC in Austenitic Stainless Steels*, Proc. 5th Int. Symp. Environmental Degradation of Materials in Nuclear Power Systems – Water Reactors, D. Cubicciotti, E. P. Simonen, and R. Gold, eds., American Nuclear Society, La Grange Park, IL, pp. 948-954 (1992).

60. A. Jenssen and L. G. Ljunberg, *Irradiation Assisted Stress Corrosion Cracking of Stainless Steel Alloys in BWR Normal Water Chemistry and Hydrogen Water Chemistry*, Proc. 6th Int. Symp. Environmental Degradation of Materials in Nuclear Power Systems - Water Reactors, R. E. Gold and E. P. Simonen, eds., The Minerals, Metals, and Materials Society, Warrendale, PA, pp. 547–553.

Distribution for NUREG/CR-4667, Vol. 18 (ANL-95/2)

Internal

W. J. Shack (45)

TIS Files

External

NRC, for distribution per R5

Libraries

ANL-E

ANL-W

Manager, Chicago Field Office, DOE

Energy Technology Division Review Committee:

H. K. Birnbaum, University of Illinois, Urbana

R. C. Buchanan, University of Cincinnati, Cincinnati

M. S. Dresselhaus, Massachusetts Institute of Technology, Cambridge, MA

B. G. Jones, University of Illinois, Urbana

C.-Y. Li, Cornell University, Ithaca, NY

S. N. Liu, Fremont, CA

R. E. Smith, SciTech, Inc., Morrisville, NC

P. L. Andresen, General Electric Corporate Research and Development, Schenectady, NY

T. A. Auten, Knolls Atomic Power Laboratory

R. G. Ballinger, Massachusetts Institute of Technology, Cambridge, MA

W. H. Bamford, Structural Materials Engineering, Westinghouse Electric Corp., Pittsburgh

S. M. Bruemmer, Battelle Pacific Northwest Laboratory

H. S. Chung, Korea Atomic Energy Research Insitiute, Daejeon, Korea

L. Coressti, ABB CE Nuclear Power, Windsor, CT

G. Cragnolino, Southwest Research Inst., San Antonio, TX

W. H. Cullen, Materials Engineering Assoc., Inc., Lanham, MD

E. D. Eason, Modeling and Computing Services, Newark, CA

M. Fox, APTECH, Tucson, AZ

D. G. Franklin, Bettis Atomic Power Laboratory

Y. S. Garud, S. Levy, Inc., Campbell, CA

F. Garzarolli, KWU, Erlangen, Germany

J. Gilman, Electric Power Research Inst., Palo Alto, CA

B. M. Gordon, General Electric Co., San Jose, CA

J. W. Halley, U. Minnesota, Minneapolis

H. E. Hanninen, Technical Research Centre of Finland, Espoo

D. Harrison, USDOE, Germantown, MD

J. Hickling, CML Capcis March Ltd., Erlangen-Tennonlohe, Germany

M. Higuchi, Ishikawajima-Harima Heavy Industries Co., Ltd., Japan

C. Hoffmann, ABB CE Nuclear Power, Windsor, CT

M. E. Indig, General Electric Co., Pleasanton, CA
H. S. Isaacs, Brookhaven National Laboratory
A. Jacobs, General Electric Co., San Jose, CA
L. James, Bettis Atomic Power Laboratory
C. Jansson, Vattenfall Energisystem, Vallingby, Sweden
R. H. Jones, Battelle Pacific Northwest Laboratory
R. L. Jones, Electric Power Research Institute, Palo Alto, CA
D. P. Jones, Bettis Atomic Power Laboratory
T. Karlsen, OECD Halden Reactor Project, Halden, Norway
C. Kim, Westinghouse Electric Corp., Pittsburgh
L. Ljungberg, ASEA-ATOM, Vasteras, Sweden
C. D. Lundin, U. Tennessee, Knoxville
D. D. Macdonald, Pennsylvania State University, University Park
T. R. Mager, Westinghouse Electric Corp., Pittsburgh
R. D. McCright, Lawrence Livermore National Laboratory
A. R. McIlree, Electric Power Research Institute, Palo Alto, CA
H. Metha, General Electric Co., San Jose, CA
D. Morgan, Pennsylvania Power and Light Co., Allentown, PA
J. L. Nelson, Electric Power Research Inst., Palo Alto, CA
D. H. Njo, Swiss Federal Nuclear Safety Inspectorate, Villigen, Switzerland
M. Prager, Materials Properties Council, New York, NY
S. Ranganath, General Electric Co., San Jose, CA
P. M. Scott, Framatome, Paris, FranceVilligen, Switzerland
J. Sedriks, Office of Naval Research, Arlington, VA
C. Shepherd, AEA Technology–Harwell Labs., Didcot, Oxon, UK
S. Smialowska, Ohio State University, Columbus
H. D. Solomon, General Electric Corporate Research and Development, Schenectady, NY
M. O. Speidel, Swiss Federal Institute of Technology, Zurich, Switzerland
D. M. Stevens, Lynchburg Research Center, Babcock & Wilcox Co., Lynchburg, VA
W. A. Van Der Sluys, Research & Development Division, Babcock & Wilcox Co., Alliance, OH
J. C. Van Duysen, Electricite de France-Research and Development Centre de Renardieres, Moret–Sur–Loing, France
E. Venerus, Knolls Atomic Power Laboratory
C. Vitanza, OECD Halden Reactor Project, Halden, Norway
G. S. Was, University of Michigan, Ann Arbor
J. R. Weeks, Brookhaven National Laboratory
D. Winkel, Teleco Oil Field Services, Meriden, CT
S. Yukawa, Boulder, CO

NRC FORM 335 (2–89) NRCM 1102, 3201, 3202

U. S. NUCLEAR REGULATORY COMMISSION

BIBLIOGRAPHIC DATA SHEET

(See instructions on the reverse)

1. REPORT NUMBER *(Assigned by NRC. Add Vol., Supp., Rev., and Addendum Numbers, if any.)*
NUREG/CR–4667, Vol. 18
ANL–95/2

2. TITLE AND SUBTITLE
Environmentally Assisted Cracking in Light Water Reactors
Semiannual Report October 1993—March 1994

3. DATE REPORT PUBLISHED
MONTH: March | YEAR: 1995

4. FIN OR GRANT NUMBER
A2212

5. AUTHOR(S)
H. M. Chung, O. K. Chopra, R. A. Erck, T. F. Kassner, W. F. Michaud, W. E. Ruther, J. E. Sanecki, W. J. Shack, and W. K. Soppet

6. TYPE OF REPORT
Technical; Semiannual

7. PERIOD COVERED *(Inclusive Dates)*
October 1993—March 1994

8. PERFORMING ORGANIZATION – NAME AND ADDRESS *(If NRC, provide Division, Office or Region, U.S. Nuclear Regulatory Commission, and mailing address; if contractor, provide name and mailing address.)*
Argonne National Laboratory
9700 South Cass Avenue
Argonne, IL 60439

9. SPONSORING ORGANIZATION – NAME AND ADDRESS *(If NRC, type "Same as above": if contractor, provide NRC Division, Office or Region, U.S. Nuclear Regulatory Commission, and mailing address.)*
Division of Engineering
Office of Nuclear Regulatory Research
U. S. Nuclear Regulatory Commission
Washington, DC 20555–0001

10. SUPPLEMENTARY NOTES

11. ABSTRACT (200 words or less)

This report summarizes work performed by Argonne National Laboratory (ANL) on fatigue and environmentally assisted cracking (EAC) in light water reactors during the six months from October 1993 to March 1994. Topics that have been investigated include fatigue of low–alloy steel used in piping, steam generators, and reactor pressure vessels; EAC of wrought and cast austenitic stainless steels (SSs); and radiation–induced segregation and irradiation–assisted stress corrosion cracking (IASCC) of Type 304 SS after accumulation of high fluence. Fatigue tests have been conducted on A302–Gr B low–alloy steel to verify whether the current predictions of modest decreases of fatigue life in simulated pressurized water reactor water are valid for high–sulfur heats that show environmentally enhanced fatigue crack growth rates. Additional crack growth data were obtained on fracture–mechanics specimens of austenitic SSs to investigate threshold stress intensity factors for EAC in high–purity oxygenated water at 289°C. Microchemical changes in high– and commercial–purity Type 304 SS specimens from control–blade absorber tubes and a control–blade sheath from operating boiling water reactors were studied by Auger electron spectroscopy and scanning electron microscopy to determine whether trace impurity elements may contribute to IASCC of solution–annealed materials.

12. KEY WORDS/DESCRIPTORS *(List words or phrases that will assist researchers in locating this report.)*
Corrosion Fatigue
Crack Growth
Irradiation–Assisted Stress Corrosion Cracking
Radiation–Induced Segregation
Stress Corrosion Cracking
A106–Gr B Steel
A302–Gr B Steel
A533–Gr B Steel
Types 316NG, 304, CF–3, CF–3M, CF–8, CF–8M Stainless Steel

13. AVAILABILITY STATEMENT
Unlimited

14. SECURITY CLASSIFICATION
(This Page)
Unclassified
(This Report)
Unclassified

15. NUMBER OF PAGES

16. PRICE